

See discussions, stats, and author profiles for this publication at: <https://www.researchgate.net/publication/324454943>

3D positive lattice walks and spherical triangles

Preprint · April 2018

DOI: 10.13140/RG.2.2.24828.64642

CITATIONS
0

READS
216

4 authors, including:



Beniamin Bogosel
École Polytechnique
25 PUBLICATIONS 108 CITATIONS

[SEE PROFILE](#)



Vincent Perrollaz
University of Tours
18 PUBLICATIONS 135 CITATIONS

[SEE PROFILE](#)

3D POSITIVE LATTICE WALKS AND SPHERICAL TRIANGLES

B. BOGOSEL, V. PERROLLAZ, K. RASCHEL, AND A. TROTIGNON

ABSTRACT. In this paper we explore the asymptotic enumeration of three-dimensional excursions confined to the positive octant. As shown in [29], both the exponential growth and the critical exponent admit universal formulas, respectively in terms of the inventory of the step set and of the principal Dirichlet eigenvalue of a certain spherical triangle, itself being characterized by the steps of the model. We focus on the critical exponent, and our main objective is to relate combinatorial properties of the step set (structure of the so-called group of the walk, existence of a Hadamard factorization, existence of differential equations satisfied by the generating functions) to geometric or analytic properties of the associated spherical triangle (remarkable angles, tiling properties, existence of an exceptional closed-form formula for the principal eigenvalue). As in general the eigenvalues of the Dirichlet problem on a spherical triangle are not known in closed form, we also develop a finite-elements method to compute approximate values, typically with ten digits of precision.

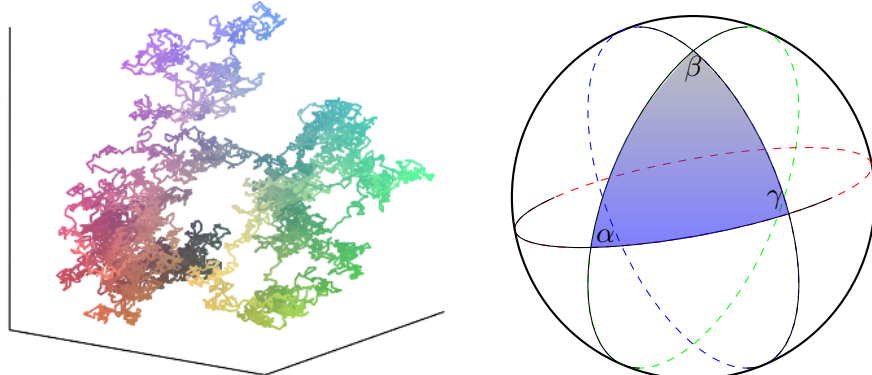


FIGURE 1. Critical exponents in the asymptotics of 3D walks (and Brownian motion) in the orthant \mathbb{N}^d can be computed in terms of the smallest eigenvalue for the Dirichlet problem on spherical triangles

Date: April 11, 2018.

1991 *Mathematics Subject Classification.* 05A15.

Key words and phrases. Enumerative combinatorics; lattice paths in the octant; asymptotic analysis; spherical geometry.

B. Bogosel: CMAP, École Polytechnique, 91120 Palaiseau, France.

V. Perrollaz: Institut Denis Poisson, Université de Tours, Parc de Grandmont, 37200 Tours, France.

K. Raschel: CNRS & Institut Denis Poisson, Université de Tours, Parc de Grandmont, 37200 Tours, France.

A. Trotignon: Institut Denis Poisson, Université de Tours, Parc de Grandmont, 37200 Tours, France & Simon Fraser University, Burnaby, BC, Canada.

This project has received funding from the European Research Council (ERC) under the European Union's Horizon 2020 research and innovation programme under the Grant Agreement No 759702.

Webpage of the article: <https://bit.ly/2J4Vf3X>.

CONTENTS

1. Introduction	3
Context	3
Asymptotics of the excursion sequence	4
Contributions of the present work	5
Brownian motion in orthants	7
Acknowledgments	7
2. Preliminaries	7
2.1. Dimension of a model	7
2.2. Group of the model	8
2.3. Hadamard structure	9
2.4. Classification of models	9
2.5. Formula for the exponent of the excursions	9
2.6. Computing the principal eigenvalue of a spherical triangle	12
3. Around the covariance matrix	13
3.1. Expression of the angles	13
3.2. Relation with the Coxeter matrix	14
3.3. Polar angles and Gram matrix	15
3.4. The reverse construction	16
4. Analysis of Hadamard models	16
4.1. (1,2)-Hadamard models	17
4.2. (2,1)-Hadamard models	19
4.3. Hadamard product of generating functions	20
5. Classification of the models and eigenvalues	21
5.1. Motivations and presentation of the results	21
5.2. Finite group case	22
5.3. Infinite group case	25
5.4. Exceptional models	27
5.5. Equilateral triangles	29
6. Numerical approximation of the critical exponent	29
6.1. Literature	29
6.2. Finite element method	30
6.3. Improving the precision using extrapolation	31
6.4. Computing exponents	32
6.5. Discussion of the computations	33
7. Miscellaneous	33
7.1. Other cones	33
7.2. Total number of walks	34
7.3. Walks in the quarter plane and spherical digons	35
7.4. Exit time from cones for Brownian motion	35
7.5. Other methods to approximate the first eigenvalue	36
7.6. Open problems	36
References	37
Appendix A. Some useful definitions from spherical geometry	39
A.1. Elementary spherical geometry	39
A.2. Some properties of the principal eigenvalue	39
Appendix B. Remarks on the exponent of mixings of two laws	41

1. INTRODUCTION

Context. The enumeration of lattice walks is an important topic in combinatorics. In addition to having various applications, it is connected to other mathematical fields such as probability theory. Latterly, lots of consideration have been given to the enumeration of walks confined to cones. We will typically be considering walks on \mathbb{Z}^d that start at the origin and consist of steps taken from \mathcal{S} , a finite subset of \mathbb{Z}^d . Most of the time we will constrain the walks in the orthant \mathbb{N}^d , with \mathbb{N} denoting the set of non-negative integers $\{0, 1, 2, \dots\}$.

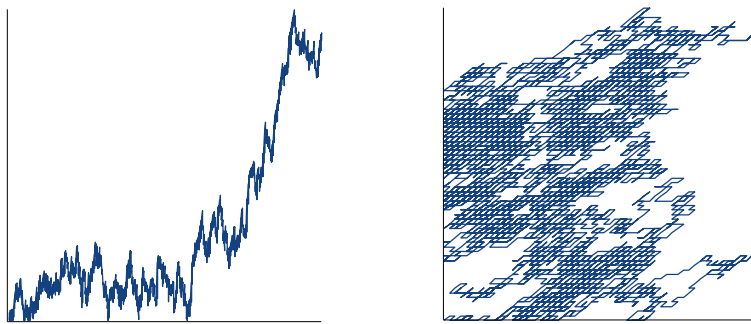


FIGURE 2. Motzkin paths in \mathbb{N} (with steps $(1, 1)$, $(1, 0)$ and $(1, -1)$) and Gessel's walks in \mathbb{N}^2 (with steps $(1, 0)$, $(1, 1)$, $(-1, 0)$ and $(-1, -1)$)

In dimension $d = 1$ (Figure 2, left) there is essentially one unique cone (the positive axis), and positive (random) walks are very well understood, see in particular [10, 5].

Following the seminal works [35, 21], many recent papers deal with the enumeration of 2D walks with prescribed steps confined to the positive quadrant (Figure 2, right). In the case of small steps (\mathcal{S} included in $\{0, \pm 1\}^2$), various results have been obtained: exact and asymptotic expressions [21, 15, 18], classification of the generating (or counting) function according to the classes rational, algebraic, D-finite (that is, solution to a linear differential equation with polynomial coefficients) [21], non-D-finite [50, 18], and even non-differentially algebraic [30].

One of the most striking results in the quadrant walks world is the following: the generating function is D-finite if and only if a certain group associated with the step set \mathcal{S} is finite. Remarkably this result connects an arithmetic property of the generating function to a geometric feature (the group, related to the symmetries of the step set). Non-convex cones (see [20] for the three quarter plane) as well as larger steps [14] have recently also been considered.

On the other hand, much less is known on 3D lattice walks confined to the non-negative octant \mathbb{N}^3 . An intrinsic difficulty lies in the number of models to handle: more than 11 millions (see [13])! (Compare with 79 quadrant models.) The first work is an empirical classification by Bostan and Kauers [15] of the models with at most five steps. Then in [13], Bostan, Bousquet-Mélou, Kauers and Melczer study models of cardinality at most six. They introduce some key concepts: the dimensionality (1D, 2D or 3D) of a model, the group of the model, the Hadamard structure (roughly speaking, it is a generalization of Cartesian products of lower dimensional models). These notions will be made precise in Section 2. Furthermore, the authors of [13] classify the models with respect to these concepts and



FIGURE 3. From left to right: the simple walk, Kreweras 3D model, a $(1, 2)$ -type Hadamard model and a $(2, 1)$ -type Hadamard model. As obviously these perspective drawings are sometimes difficult to read, we will prefer the cross-section views of the step sets as on Figure 4. These pictures are courtesy of Alin Bostan



FIGURE 4. For each model, the first diagram shows steps of the form $(i, j, -1)$, the second the steps $(i, j, 0)$, and the third the steps $(i, j, 1)$. The models are the same ones as on Figure 3. These cross-section views were first proposed in [15, 13]

compute, in various cases (but only in presence of a finite group), the generating function

$$O(x, y, z; t) = \sum_{i,j,k,n \geq 0} o(i, j, k; n) x^i y^j z^k t^n, \quad (1)$$

where $o(i, j, k; n)$ is the number of n -step walks in the octant starting at the origin $(0, 0, 0)$ and ending at position (i, j, k) . In majority, the techniques used in [13] to solve finite group models are the algebraic kernel method and computer algebra (using the guessing-and-proving paradigm).

The classification (in particular with respect to the finiteness of the group and the Hadamard structure) of the 3D small step models with arbitrary cardinality is pursued in the articles [2, 31, 58, 48]. Table 2 reproduces this classification.

Asymptotics of the excursion sequence. Let us finally mention the article [29] by Denisov and Wachtel, which is fundamental for our study. It proves in a great level of generality the following asymptotics for the excursion sequence $o_{A \rightarrow B}(n)$, i.e., the number of n -step walks in the octant starting (resp. ending) at $A \in \mathbb{N}^3$ (resp. $B \in \mathbb{N}^3$): if A and B are far enough from the boundary, as $n \rightarrow \infty$,

$$o_{A \rightarrow B}(pn) = \varkappa(A, B) \cdot \rho^{pn} \cdot n^{-\lambda} \cdot (1 + o(1)), \quad (2)$$

where $\varkappa(A, B) > 0$ is some constant, $\rho \in (0, |\mathcal{S}|]$ is the exponential growth, $\lambda > 0$ is the critical exponent and p is the period of the model, i.e.,

$$p = \gcd\{n \in \mathbb{N} : o_{A \rightarrow B}(n) > 0\}. \quad (3)$$

The asymptotics (2) is proved in [29] in the aperiodic case ($p = 1$) and commented in [33, 14] for periodic models ($p > 1$). For the exact hypotheses and a discussion, see Theorem 3 in Section 2.5 and the comments following the statement.

The quantities ρ and λ in (2) are computed in [29]. First, ρ is the global minimum on \mathbb{R}_+^d of the inventory (or characteristic polynomial)

$$\chi_{\mathcal{S}}(x, y, z) = \chi(x, y, z) = \sum_{(i,j,k) \in \mathcal{S}} x^i y^j z^k \quad (4)$$

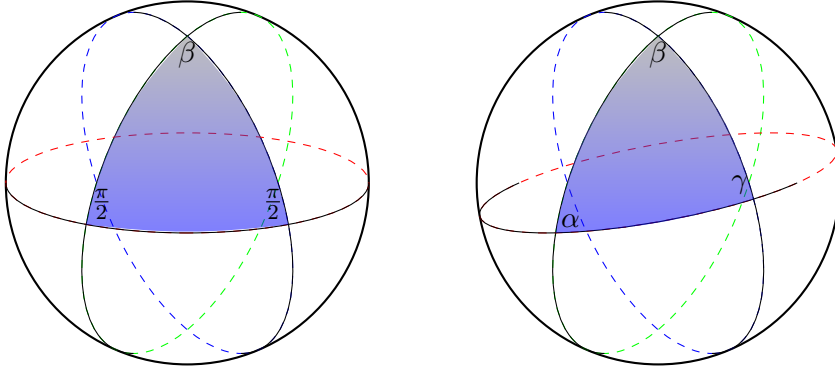


FIGURE 5. On the left: a particular spherical triangle with two right angles (these triangles will eventually correspond to Hadamard models). On the right: a generic triangle with angles α, β, γ

and is thus well understood and easily computed. On the other hand, λ is much more mysterious and challenging: it is characterized in [29] as the smallest eigenvalue of a certain Dirichlet problem on a spherical triangle.

Concerning the algebraic nature of the 3D generating function (1), a few results are known: in the finite group cases solved in [13], the generating function is always D-finite. On the other hand, the article [31] proves that for some 3D model with dimensionality 2 (in the sense of Definition 1), the excursion generating function $O(0, 0, 0; t)$ is non-D-finite, by looking at the asymptotic behavior of the excursion sequence and showing that λ in (2) is non-rational, extending the work [18]. A very exciting question is (that unfortunately we won't solve): does there exist a 3D finite group model with a non-D-finite generating function (1)? Typically, the 3D Kreweras model of Figure 3 is a candidate!

Contributions of the present work. In this article we focus on the asymptotics (2) of the numbers of excursions and assume that:

- (H) The step set \mathcal{S} is not included in any half-space $x^+ = \{y \in \mathbb{R}^d : \langle x, y \rangle \geq 0\}$, with $x \in \mathbb{R}^d \setminus \{0\}$.

Applying the results of [29] (see in particular Equation (12) there) readily shows, under the hypothesis (H), the following expression for the critical exponent:

$$\lambda = \sqrt{\lambda_1 + \frac{1}{4}} + 1, \quad (5)$$

where λ_1 is the smallest eigenvalue of the Dirichlet problem

$$\begin{cases} \Delta_{\mathbb{S}^2} m = -\Lambda m & \text{in } T, \\ m = 0 & \text{in } \partial T, \end{cases} \quad (6)$$

$T = T(\alpha, \beta, \gamma)$ being a spherical triangle (see Figure 5 for an illustration), which can be computed algorithmically (and easily) in terms of the model \mathcal{S} , see Theorem 3 for a precise statement.

In **Section 2** we recall all needed definitions and first properties of 3D models. Results in that section come from [29, 13, 2, 48]. Let us now present our main contributions.

- **Section 3** gives the exact value of the angles. We prove that the cosine matrix of the angles is strongly related to the Coxeter matrix of the group, and can also be interpreted as a Gram matrix.

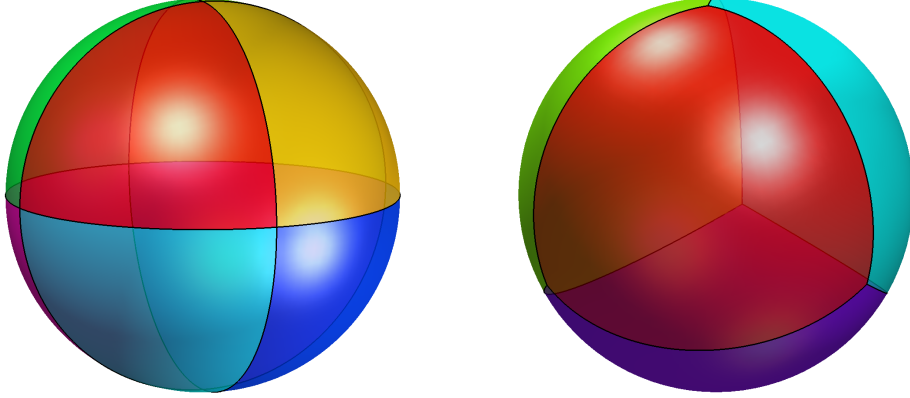


FIGURE 6. Left: tiling of the sphere by equilateral triangles with right angles, corresponding to the simple walk. Right: the tetrahedral partition of the sphere, corresponding to Kreweras 3D model. See Figure 11 for further examples of tilings

- We then show that the spherical triangle captures a lot of combinatorial information about the model from which it is constructed, in the following sense:
 - Finite group models correspond to triangular tilings of the sphere \mathbb{S}^2 . The simplest example is the simple walk with jumps

$$\mathcal{S} = \{(\pm 1, 0, 0), (0, \pm 1, 0), (0, 0, \pm 1)\},$$

see Figure 4 (leftmost). Its triangle has three right angles, namely $\alpha = \beta = \gamma = \frac{\pi}{2}$ on Figures 5 and 6. A second example is 3D Kreweras model, with step set

$$\mathcal{S} = \{(-1, 0, 0), (0, -1, 0), (0, 0, -1), (1, 1, 1)\},$$

see Figure 4 (left). The associated triangle is also equilateral, with angles $\frac{2\pi}{3}$, this corresponds to the tetrahedral tiling of the sphere. See Figure 6.

- Hadamard models have birectangular triangles (i.e., with two right angles), as on Figure 5, left. Finite group (resp. infinite) Hadamard models correspond to angles β such that $\frac{\pi}{\beta} \in \mathbb{Q}$ (resp. $\frac{\pi}{\beta} \notin \mathbb{Q}$).
- Although we won't consider these issues here, let us mention that we can also see the dimensionality on the triangle. In the case of 2D models, the triangles degenerate into a spherical digon, see Section 7.3 (in particular Figure 18).
- **Section 4:** Our next result is the study of Hadamard models (mostly with infinite group, as finite group Hadamard walks are solved in [13]). They are quite special for combinatorial reasons, as explained in [13], but also for the Laplacian: to the best of our knowledge, their birectangular triangles are the only ones (with the exception of the tiling triangles described in Lemma 25) for which one can compute the first eigenvalue! (See (17).)

We deduce the critical exponent λ and show that (most of the) infinite group Hadamard models are non-D-finite. This is the first result on the non-D-finiteness of truly 3D models.

- **Section 5:** We classify the models with respect to their triangle and the associated principal eigenvalue, and compare our results with the classification in terms of the group and the Hadamard property obtained in [13, 48]. We exhibit some

exceptional models, which do not have the Hadamard property but for which, remarkably, one can compute an explicit form for the eigenvalue; this typically leads to non-D-finiteness results.

- **Section 6:** Our last result is about generic infinite group models. Even if no closed-form formula exists for λ_1 , we may consider λ_1 as a *special function* of the triangle T (or equivalently of its angles α, β, γ), and with numerical analysis methods, obtain approximations of this function when evaluated at particular values. The techniques developed in Section 6 are completely different from the rest of the paper.

Notice that for some cases, approximate values of the critical exponents have been found by Bostan and Kauers [15], Bacher, Kauers and Yatchak [2], and Guttman [42]. In these three articles the method is to compute a certain amount of terms of the generating function $O(0, 0, 0; t)$ and then to estimate the exponents via different ideas. Our technique has the advantage of being applicable to any spherical triangle, not necessarily related to a 3D model.

Section 7 proposes various extensions and remarks. Finally, the brief **Appendix A** gathers some elementary facts on spherical geometry.

Brownian motion in orthants. To conclude this introduction, let us emphasize that all results that we obtain for discrete random walks admit continuous analogues and can be used to estimate exit times from cones Brownian motion, see Section 7.4. In the literature, one can also find applications to the Brownian pursuit [53, 54].

Acknowledgments. This work has benefited from discussions with many colleagues. We in particular warmly thank M. Kauers for interesting discussions and for sharing with us a complete and very precise classification (and many other data) about 3D walks. Many thanks also to V. Beck, A. Bostan, M. Bousquet-Mélou, S. Cantat, M. Dauge, T. Guttman, L. Hillairet, A. Lejay, S. Mustapha and B. Salvy. This project has received funding from the European Research Council (ERC) under the European Union’s Horizon 2020 research and innovation programme under the Grant Agreement No 759702.

2. PRELIMINARIES

In this section we introduce key concepts to study 3D walks. We are largely inspired by the paper [13], to which we borrowed Section 2.1 (dimension of a model), Section 2.2 (group of a model) and Section 2.3 (Hadamard structure). The thorough classification of Section 2.4 is done in the papers [2, 48] and the fundamental asymptotic result of Section 2.5 can be found in [29]. We follow the notations of [13].

2.1. Dimension of a model. Let \mathcal{S} be a model. A walk of length n taking its steps in \mathcal{S} can be viewed as a word $w = w_1 w_2 \dots w_n$ made up of letters of \mathcal{S} . For $s \in \mathcal{S}$, let a_s be the multiplicity (i.e., the number of occurrences) of s in w . Then w ends in the positive octant if and only if the following three linear inequalities hold:

$$\sum_{s \in \mathcal{S}} a_s s_x \geq 0, \quad \sum_{s \in \mathcal{S}} a_s s_y \geq 0, \quad \sum_{s \in \mathcal{S}} a_s s_z \geq 0, \quad (7)$$

where $s = (s_x, s_y, s_z)$. Of course, the walk w remains in the octant if the multiplicities observed in each of its prefixes satisfy these inequalities.

Definition 1 ([13]). *Let $d \in \{0, 1, 2, 3\}$. A model \mathcal{S} is said to have dimension at most d if there exist d inequalities in (7) such that any $|\mathcal{S}|$ -tuple $(a_s)_{s \in \mathcal{S}}$ of non-negative integers*

satisfying these d inequalities satisfies in fact the three ones. We define accordingly models of dimension (exactly) d .

In what follows we will be principally considering models of dimension 3, and in fact only a subclass of them: most of the time we will assume the hypothesis (H).

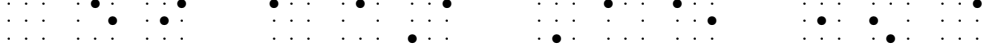


FIGURE 7. Four-step models of respective dimension 0, 1, 2 and 3. These examples are borrowed from [13]

2.2. Group of the model. Write the inventory (or characteristic polynomial) χ in (4) as (we take the same notations as in [13])

$$\begin{aligned}\chi(x, y, z) &= \bar{x}A_-(y, z) + A_0(y, z) + xA_+(y, z) \\ &= \bar{y}B_-(x, z) + B_0(x, z) + yB_+(x, z) \\ &= \bar{z}C_-(x, y) + C_0(x, y) + zC_+(x, y),\end{aligned}$$

where $\bar{x} = \frac{1}{x}$, $\bar{y} = \frac{1}{y}$ and $\bar{z} = \frac{1}{z}$. If \mathcal{S} is 3-dimensional then it has a positive step in each direction and A_+ , B_+ and C_+ are all non-zero. The group of \mathcal{S} is the group $G = \langle \phi, \psi, \tau \rangle$ of birational transformations of the variables $[x, y, z]$ generated by the following three involutions:

$$\left\{ \begin{array}{l} \phi([x, y, z]) = \left[\bar{x} \frac{A_-(y, z)}{A_+(y, z)}, y, z \right], \\ \psi([x, y, z]) = \left[x, \bar{y} \frac{B_-(x, z)}{B_+(x, z)}, z \right], \\ \tau([x, y, z]) = \left[x, y, \bar{z} \frac{C_-(x, y)}{C_+(x, y)} \right]. \end{array} \right. \quad (8)$$

The classification of the models according to the (in)finiteness of the group is known, see Table 2. Let us also reproduce Table 1 of [48]:

Group	Number of models	Group	Number of models
$G_1 = \langle a, b, c \mid a^2, b^2, c^2 \rangle$	10,759,449	$G_7 = \langle a, b, c \mid a^2, b^2, c^2, (ab)^4 \rangle$	82
$G_2 = \langle a, b, c \mid a^2, b^2, c^2, (ab)^2 \rangle$	84,241	$G_8 = \langle a, b, c \mid a^2, b^2, c^2, (ab)^3, (bc)^3 \rangle$	30
$G_3 = \langle a, b, c \mid a^2, b^2, c^2, (ac)^2, (ab)^2 \rangle$	58,642	$G_9 = \langle a, b, c \mid a^2, b^2, c^2, acbacbabc \rangle$	20
$G_4 = \langle a, b, c \mid a^2, b^2, c^2, (ac)^2, (ab)^3 \rangle$	1,483	$G_{10} = \langle a, b, c \mid a^2, b^2, c^2, (ab)^3, (cbca)^2 \rangle$	8
$G_5 = \langle a, b, c \mid a^2, b^2, c^2, (ab)^3 \rangle$	1,426	$G_{11} = \langle a, b, c \mid a^2, b^2, c^2, (ca)^3, (ab)^4, (babc)^2 \rangle$	8
$G_6 = \langle a, b, c \mid a^2, b^2, c^2, (ac)^2, (ab)^4 \rangle$	440	$G_{12} = \langle a, b, c \mid a^2, b^2, c^2, (ab)^4, (ac)^4 \rangle$	4

TABLE 1. Various infinite groups associated to 3D models. Notice that the presentations of the groups are not certified: though highly unlikely, it is not excluded [48] that further relations exist, but then involving more than 400 generators a, b, c . Remark that with the exception of G_9 , G_{10} and G_{11} , all groups are Coxeter groups. Most of the time, but not systematically, one can take $a = \phi$, $b = \psi$ and $c = \tau$

2.3. Hadamard structure. Hadamard models are introduced in [13] (see in particular Section 5 there). These are 3-dimensional models which can be reduced to the study of a pair of models, one in \mathbb{Z} and one in \mathbb{Z}^2 , using Hadamard product of generating functions (more is to come in Section 4.3).

There are two types of Hadamard models: the $(1, 2)$ -type and the $(2, 1)$ -type. More generally, in arbitrary dimension d there is the notion of (D, δ) -Hadamard model, with $D + \delta = d$, see [13, Section 5.2]. Back to the dimension 3, the $(1, 2)$ -type corresponds to models for which the inventory (4) can be written under the form

$$\chi(x, y, z) = U(x) + V(x)T(y, z). \quad (9)$$

The $(2, 1)$ -type corresponds to models for which the inventory can be written as

$$\chi(x, y, z) = U(x, y) + V(x, y)T(z). \quad (10)$$

The number of Hadamard models (with the additional information on the type) can be found on Table 2.

For each type, an example is presented on Figure 4. For the $(2, 1)$ -type we have taken $U(x, y) = x + \bar{x} + y + \bar{y}$ (the 2D simple walk, see Figure 8), $V(x, y) = x + x\bar{y} + \bar{x}\bar{y} + \bar{x}y + y$ (a scarecrow model, see again Figure 8) and $T(z) = z + \bar{z}$.

For the $(1, 2)$ -type we have $\chi(x, y, z) = U(z) + V(z)T(x, y)$ (permutation of the variables in the definition (9)), with $U(z) = z + \bar{z}$, $V(z) = z + 1 + \bar{z}$ and $T(x, y)$ the generating function of the same scarecrow model as above.

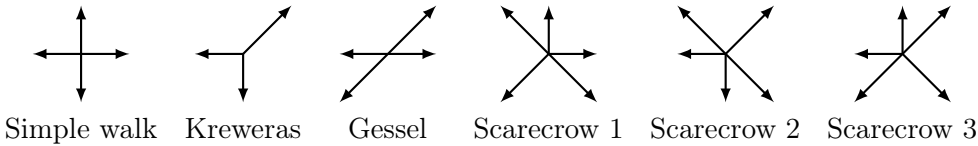


FIGURE 8. Some 2D models, which can be used to construct 3D Hadamard models. The three scarecrows are named after [18, Fig. 1]

Hadamard models generalize Cartesian products of walks: Cartesian products (or equivalently independent random walks in the probabilistic framework) correspond to taking $U(x) = 0$ in (9), or $U(x, y) = 0$ in (10). Notice that Hadamard models in dimension 2 are always D-finite [14], even with large steps.

2.4. Classification of models. Before stating the precise classification of the models we need a final concept, namely, the notion of equivalent models: two models are said to be equivalent if they only differ by a permutation of the step coordinates, or if they only differ by unused steps, that is, steps that are never used in a walk confined to the octant.

Proposition 2.5 of [13] computes the number of models having dimension 2 or 3, no unused step, and counted up to permutations of the coordinates, ending up with the number 11,074,225 on Table 2.

2.5. Formula for the exponent of the excursions. We now explain that the exponent λ in (2) is directly related to the smallest eigenvalue of a certain Dirichlet problem on a spherical triangle. Let us start with a simple definition:

Definition 2 ([9]). *A spherical triangle on \mathbb{S}^2 is a triple (x, y, z) of points of \mathbb{S}^2 that are linearly independent as vectors in \mathbb{R}^3 . We denote it by $\langle x, y, z \rangle$.*

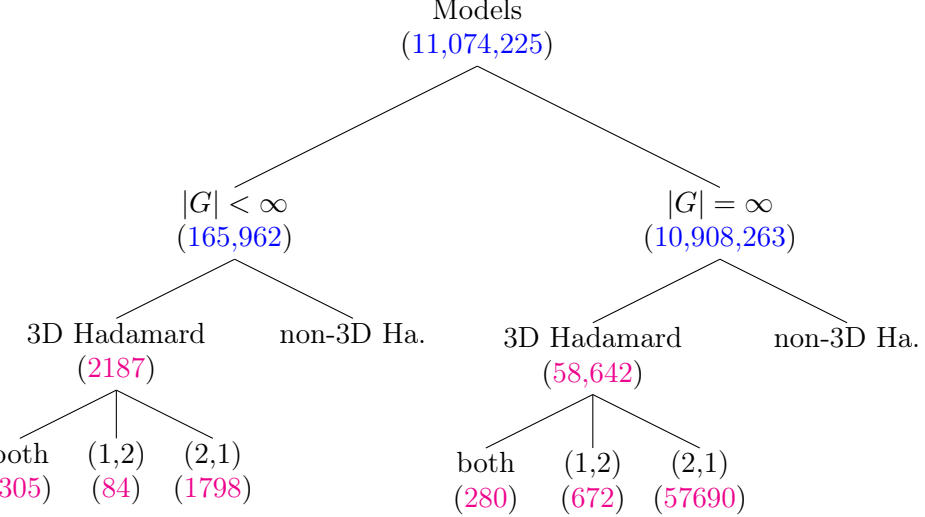


TABLE 2. Classification of 3D walks (of dimension 2 and 3) according to the finiteness of the group and the Hadamard property [48]. The numbers of (non-)Hadamard models refer exclusively to dimension 3 models. Hence among the non-3D Hadamard models one can find models of dimensionality 2 having a (degenerate) Hadamard decomposition. A model labeled “both” is simultaneously (1, 2)-type and (2, 1)-type Hadamard. The total number of models is computed in [13], the number of (in)finite groups in [13, 31, 48] and the refined statistics on 3D Hadamard models in [47]

See examples on Figures 5 and 6. The points x, y, z are called the vertices of $\langle x, y, z \rangle$. By the sides of $\langle x, y, z \rangle$ we mean the arcs of great circle determined by (x, y) , (y, z) and (z, x) .

Theorem 3 ([29]). *Let \mathcal{S} be a step set satisfying to (H) and irreducible. Let χ be its inventory (4). The system of equations*

$$\frac{\partial \chi}{\partial x} = \frac{\partial \chi}{\partial y} = \frac{\partial \chi}{\partial z} = 0 \quad (11)$$

admits a unique solution, denoted by (x_0, y_0, z_0) . Define

$$a = \frac{\frac{\partial^2 \chi}{\partial x \partial y}}{\sqrt{\frac{\partial^2 \chi}{\partial x^2} \cdot \frac{\partial^2 \chi}{\partial y^2}}}(x_0, y_0, z_0), \quad b = \frac{\frac{\partial^2 \chi}{\partial x \partial z}}{\sqrt{\frac{\partial^2 \chi}{\partial x^2} \cdot \frac{\partial^2 \chi}{\partial z^2}}}(x_0, y_0, z_0), \quad c = \frac{\frac{\partial^2 \chi}{\partial y \partial z}}{\sqrt{\frac{\partial^2 \chi}{\partial y^2} \cdot \frac{\partial^2 \chi}{\partial z^2}}}(x_0, y_0, z_0) \quad (12)$$

and introduce the covariance matrix

$$\text{cov} = \begin{pmatrix} 1 & a & b \\ a & 1 & c \\ b & c & 1 \end{pmatrix}. \quad (13)$$

Let S denote a square root of the covariance matrix, namely

$$\text{cov} = S S^\dagger. \quad (14)$$

Consider the spherical triangle $T = (S^{-1}\mathbb{R}_+^3) \cap \mathbb{S}^2$. Let λ_1 be the smallest eigenvalue of the Dirichlet problem (6). Then for A and B far enough from the boundary, the asymptotics

(2) of the number of excursions going from A to B holds, where

$$\rho = \min_{(0,\infty)^3} \chi \quad (15)$$

and the critical exponent λ in (2) is given by (5).

Before sketching the proof of Theorem 3 we comment on its hypotheses.

- First, under (H) the characteristic polynomial is strictly convex on $(0,\infty)^3$ and hence there is a unique global minimizing point (x_0, y_0, z_0) , which satisfies to (11).
- The covariance matrix (13) is positive definite, this is a direct consequence of (H) (the rank of the covariance matrix describes the dimension of the subspace in which the random walks evolves).
- The matrix S^{-1} has full rank and hence $T = (S^{-1}\mathbb{R}_+^3) \cap \mathbb{S}^2$ is a spherical triangle (see our Definition 2), bounded by the three great-circle arcs $(S^{-1}e_i) \cap \mathbb{S}^2$, with e_i denoting the i -th vector of the canonical basis.
- The choice of the square root in (14) is not relevant: if $\text{cov} = S_1 S_1^\top = S_2 S_2^\top$ then obviously $S_1 = M S_2$, where M is an orthogonal matrix, and the two associated spherical triangles are isomorphic (and in particular they have the same angles).
- The boundary of the spherical triangle is obviously piecewise infinitely differentiable. Under this assumption, the spectrum of the Laplacian for the Dirichlet problem (6) is discrete (see [22, p. 169]), of the form $0 < \lambda_1 < \lambda_2 \leq \lambda_3 \leq \dots$.
- The irreducibility hypothesis means that for any two points in the space \mathbb{Z}^3 , there exists a path connecting these points.
- The asymptotics (2) is proved in [29] under the assumption that the walk is strongly aperiodic (see the lattice assumption in [29, p. 999]), i.e., irreducible and aperiodic in the sense of the Markov chains. The aperiodicity is defined by $p = 1$ in (3). Two remarks should be done:
 - As explained in [14], an extra-assumption (namely, a reachability condition) has to be done. There is indeed in [14] the example of a 2D walk which is strongly aperiodic but such that no excursion to the origin is possible, due to the (ad hoc) particular configuration of the jumps. We could easily construct a 3D analogue such that $o(0, 0, 0; n) = 0$ for all n .
 - The second point is about periodic models ($p > 1$ in (3)), which stricto sensu are not covered by [29]. It is briefly mentioned in [33] that the main asymptotics (2) still holds true. A detailed discussion of the periodic case may be found in [14].

As our point is not to state Theorem 3 at the greatest level of generality, we have stated it under rather strong hypotheses, namely that A and B are far enough from the boundary (this is sufficient for the reachability condition).

Sketch of the proof of Theorem 3. This proof follows a certain number of steps that we now briefly recall. For more details we refer to the presentation of [18] (see Section 2.3 there).

- *Probabilistic interpretation:* Following Denisov and Wachtel [29, Sec. 1.5], the main idea is to write the number of excursions (see (1)) as a local probability for a random walk, namely,

$$o(i, j, k; n) = |\mathcal{S}|^n \mathbb{P} \left[\sum_{\ell=1}^n (X(\ell), Y(\ell), Z(\ell)) = (i, j, k), \tau > n \right], \quad (16)$$

where $\{(X(\ell), Y(\ell), Z(\ell))\}$ are i.i.d copies of a random variable (X, Y, Z) having uniform law on the step set \mathcal{S} , i.e., for each $s \in \mathcal{S}$, $\mathbb{P}[(X, Y, Z) = s] = 1/|\mathcal{S}|$, and where τ is the first hitting time of the translated cone $(\mathbb{N} \cup \{-1\})^3$. At the end we shall apply the local limit theorem [29, Thm 6] for random walks in cones. The latter theorem gives the asymptotics of (16) for normalized random walks, in the sense that the increments of the random walks should have no drift and a covariance matrix equal to the identity.

- *Removing the drift:* It is rather standard to perform an exponential change of measure so as to remove the drift of a random variable (this is known as the Cramér transform). Define the triplet (X_1, Y_1, Z_1) by (with $s = (s_1, s_2, s_3) \in \mathcal{S}$)

$$\mathbb{P}[(X_1, Y_1, Z_1) = s] = \frac{x_0^{s_1} y_0^{s_2} z_0^{s_3}}{\chi(x_0, y_0, z_0)}.$$

Under our hypothesis (H), the drift of (X_1, Y_1, Z_1) is zero if and only if (x_0, y_0, z_0) is solution to (11), which we now assume. (See Appendix B for similar computations in 2D.)

- *Covariance identity:* We first normalize the variables by

$$(X_2, Y_2, Z_2) = \left(\frac{X_1}{\sqrt{\mathbb{E}[X_1^2]}}, \frac{Y_1}{\sqrt{\mathbb{E}[Y_1^2]}}, \frac{Z_1}{\sqrt{\mathbb{E}[Z_1^2]}} \right),$$

so that the variances of the coordinates are 1, and more generally the covariance matrix of (X_2, Y_2, Z_2) is given by (13). Writing $\text{cov} = SS^\top$ as in (14) and

$$\begin{pmatrix} X_3 \\ Y_3 \\ Z_3 \end{pmatrix} = S^{-1} \begin{pmatrix} X_2 \\ Y_2 \\ Z_2 \end{pmatrix},$$

we obtain that (X_3, Y_3, Z_3) has an identity covariance matrix, since $S^{-1}\text{cov}(S^{-1})^\top$ is the identity. If (X, Y, Z) is defined in the octant \mathbb{R}_+^3 , then (X_3, Y_3, Z_3) takes its values in the cone $S^{-1}\mathbb{R}_+^3$.

- *Conclusion:* Remarkably, the probability on the right-hand side of (16) can be expressed in terms of the random walk with increments (X_3, Y_3, Z_3) . For instance, for (i, j, k) equal to the origin,

$$\begin{aligned} \mathbb{P} \left[\sum_{\ell=1}^n (X(\ell), Y(\ell), Z(\ell)) = (0, 0, 0), \tau > n \right] = \\ \left(\frac{\chi(x_0, y_0, z_0)}{|\mathcal{S}|} \right)^n \mathbb{P} \left[\sum_{\ell=1}^n (X_3(\ell), Y_3(\ell), Z_3(\ell)) = (0, 0, 0), \tau_3 > n \right], \end{aligned}$$

with τ_3 denoting the exit time from the cone $S^{-1}\mathbb{R}_+^3$. Using (16) and applying [29, Thm 6] finally gives the result stated in (3).

2.6. Computing the principal eigenvalue of a spherical triangle.

It turns out that there are a very few spherical triangles (and more generally, a few domains on the sphere, see Section 7.1) for which we can explicitly compute the first eigenvalue λ_1 of the Dirichlet problem (6). As a matter of comparison, let us recall that (to the best of our knowledge, see also [8]) there does not exist in general a closed-form expression for the analogous problem for flat triangles!

Back to the spherical triangles, there essentially exists a unique case for which an explicit expression for λ_1 is known: the case of two angles $\frac{\pi}{2}$ as on Figure 5 (these triangles are

sometimes called birectangular). Then according to [57, Eq. (36)] (or [56, Sec. IV]) the smallest eigenvalue is

$$\lambda_1 = \left(\frac{\pi}{\beta} + 1 \right) \left(\frac{\pi}{\beta} + 2 \right). \quad (17)$$

Let us give three relevant cases of application in the range of formula (17):

- The 3D simple random walk (Figure 4): then $\beta = \frac{\pi}{2}$ and $\lambda_1 = 12$, which with (5) corresponds to $\lambda = \frac{9}{2}$ (in accordance with the intuition $3 \times \frac{3}{2}$, i.e., three independent positive 1D excursions).
- More generally, finite group Hadamard models. They correspond to $\beta \in \pi\mathbb{Q}$. Geometrically, they represent tiling groups of the sphere. See Section 5 for more details.
- Last but not least, all Hadamard models, even with infinite group (typically $\beta \notin \pi\mathbb{Q}$); see Section 4.

3. AROUND THE COVARIANCE MATRIX

3.1. Expression of the angles. It is noteworthy that the angles of the spherical triangle appearing in the main Theorem 3 are totally explicit (and quite simple) in terms of the correlation coefficients a, b and c defined in (12).

Lemma 4. *Let α, β, γ be the angles of the spherical triangle T defined in Theorem 3, and a, b, c in (12). One has*

$$\alpha = \arccos(-a), \quad \beta = \arccos(-b), \quad \gamma = \arccos(-c). \quad (18)$$

In words, Lemma 4 says that given a 3D random walk, the correlation coefficients a, b and c should be computed as in (12), and the arccosine of their opposite value gives the angles of the triangle. Four remarks should be done:

- It is easily seen that the correlation coefficients a, b and c of Lemma 4 are algebraic numbers. We can use the exact same algorithmic computations as in [18, Sec. 2.4.1] to deduce their minimal polynomial.
- The formulas given in Lemma 4 are the most natural generalization of the 2D situation, where by [18] the spherical triangle is replaced by a wedge of opening angle $\arccos(-c)$, see Figure 9.
- The matrix cov in (13) may be rewritten as the cosine matrix

$$\begin{pmatrix} 1 & -\cos(\gamma) & -\cos(\beta) \\ -\cos(\gamma) & 1 & -\cos(\alpha) \\ -\cos(\beta) & -\cos(\alpha) & 1 \end{pmatrix}. \quad (19)$$

- If two of the three correlation coefficients a, b and c are equal to 0, then the spherical triangle is birectangular.

Proof of Lemma 4. Let cov be the matrix defined in (13). We easily obtain the Cholesky decomposition $\text{cov} = LL^\top$, with

$$L = \begin{pmatrix} 1 & 0 & 0 \\ a & \sqrt{1-a^2} & 0 \\ b & \frac{c-ab}{\sqrt{1-a^2}} & \frac{\sqrt{1-a^2-b^2-c^2+2abc}}{\sqrt{1-a^2}} \end{pmatrix}. \quad (20)$$

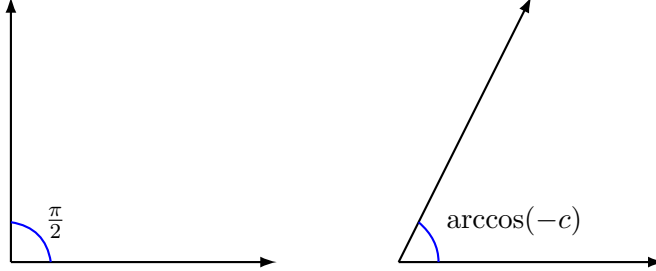


FIGURE 9. After decorrelation of a 2D random walk, the quarter plane (left) becomes a wedge of opening $\arccos(-c)$ (right), where c is the correlation coefficient of the driftless model

One deduces that

$$L^{-1} = \begin{pmatrix} 1 & 0 & 0 \\ \frac{-a}{\sqrt{1-a^2}} & \frac{1}{\sqrt{1-a^2}} & 0 \\ \frac{ac-b}{\sqrt{1-a^2}\sqrt{1-a^2-b^2-c^2+2abc}} & \frac{ab-c}{\sqrt{1-a^2}\sqrt{1-a^2-b^2-c^2+2abc}} & \frac{\sqrt{1-a^2}}{\sqrt{1-a^2-b^2-c^2+2abc}} \end{pmatrix}. \quad (21)$$

Denoting by (e_1, e_2, e_3) the canonical basis of \mathbb{R}^3 , the three points defining the triangle are

$$x = \frac{L^{-1}e_1}{\|L^{-1}e_1\|}, \quad y = \frac{L^{-1}e_2}{\|L^{-1}e_2\|}, \quad z = \frac{L^{-1}e_3}{\|L^{-1}e_3\|}.$$

Setting

$$x_y = \frac{y - \langle x, y \rangle x}{\|y - \langle x, y \rangle x\|}$$

and x_z, y_x, y_z, z_x, z_y similarly, we have by [9, 18.6.6] (giving the formulas for the angles of the triangle $\langle x, y, z \rangle$)

$$\alpha = \arccos\langle x_y, x_z \rangle, \quad \beta = \arccos\langle y_z, y_x \rangle, \quad \gamma = \arccos\langle z_x, z_y \rangle.$$

To conclude the proof it is enough to do the above computations in terms of a, b and c . \square

Notice that the above expression of L in terms of a, b and c is particularly simple, and thus the proof of Lemma 4 is easily obtained. This is a little miracle in the sense that the equation $\text{cov} = SS^\top$ is complicated: trying to solve it with S a symmetric matrix is less intrinsic.

3.2. Relation with the Coxeter matrix. Assume that there exists a representation of the group G of Section 2.2 as

$$G = \langle \mathbf{a}, \mathbf{b}, \mathbf{c} \mid \mathbf{a}^2, \mathbf{b}^2, \mathbf{c}^2, (\mathbf{ab})^{m_{ab}}, (\mathbf{ac})^{m_{ac}}, (\mathbf{bc})^{m_{bc}} \rangle,$$

with $m_{ab} = \infty$ if there is no relation between \mathbf{a} and \mathbf{b} , and similarly for m_{ac} and m_{bc} . (It is not always possible to represent the group G as above, see Table 1.) Following Bourbaki [19] we introduce the two matrices

$$\begin{pmatrix} 1 & m_{ab} & m_{ac} \\ m_{ab} & 1 & m_{bc} \\ m_{ac} & m_{bc} & 1 \end{pmatrix} \quad \text{and} \quad \begin{pmatrix} 1 & -\cos\left(\frac{\pi}{m_{ab}}\right) & -\cos\left(\frac{\pi}{m_{ac}}\right) \\ -\cos\left(\frac{\pi}{m_{ab}}\right) & 1 & -\cos\left(\frac{\pi}{m_{bc}}\right) \\ -\cos\left(\frac{\pi}{m_{ac}}\right) & -\cos\left(\frac{\pi}{m_{bc}}\right) & 1 \end{pmatrix}. \quad (22)$$

The first one is called the Coxeter matrix, see Def. 4 in [19, Ch. IV]. The second one is used in [19] to define a quadratic form, whose the property of being non-degenerate eventually characterizes the finiteness of the group G , see Thm 2 in [19, Ch. V].

Our point here is to remark the strong link between the covariance matrix (19) and the matrix on the right-hand side of (22). This interpretation of the covariance matrix as a Coxeter matrix in particular illustrates how natural these cosine matrices are.

There are, however, two differences between the matrices (19) and (22). The first one is that in the infinite group case, all non-diagonal coefficients of the matrix (19) are in $(-1, 1)$, while if there is no relation between \mathbf{a} and \mathbf{b} (say), then $m_{ab} = \infty$ and $-\cos(\frac{\pi}{m_{ab}}) = -1$. See [27] for a rather general study of cosine matrices (19) (in arbitrary dimension).

The second difference is about the finite group case. Take any two step sets which are obtained the one from the other by a reflection (see Figure 10 for an example). Then the group has the exact same structure and thus the matrix of [19] is unchanged. On the other hand, the matrix (19) changes after a reflection (Kreweras on the left, reflected Kreweras on the right):

$$\begin{pmatrix} 1 & \frac{1}{2} & \frac{1}{2} \\ \frac{1}{2} & 1 & \frac{1}{2} \\ \frac{1}{2} & \frac{1}{2} & 1 \end{pmatrix} \quad \text{and} \quad \begin{pmatrix} 1 & -\frac{1}{2} & -\frac{1}{2} \\ -\frac{1}{2} & 1 & \frac{1}{2} \\ -\frac{1}{2} & \frac{1}{2} & 1 \end{pmatrix}.$$

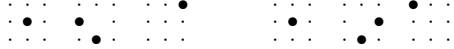


FIGURE 10. On the left, Kreweras 3D model. On the right, the reflection of Kreweras 3D with respect to the x -axis, which can be thought of as a 3D tandem model

3.3. Polar angles and Gram matrix. It is also possible to compute the angles between the three segments connecting the origin to the vertices of the triangle $\langle x, y, z \rangle$. These angles may also be interpreted as the lengths $A = \overline{yz}$, $B = \overline{xz}$ and $C = \overline{xy}$ of the sides of the triangle, see [9, 18.6.6]. Finally, they are strongly related to the angles of the polar triangle (see Definition 20): by [9, 18.6.12.2] they are the complements to π of the polar angles.

Lemma 5. *Let O denote the origin $(0, 0, 0)$. The angles between the vectors \vec{Ox} , \vec{Oy} and \vec{Oz} are given by*

$$A = \arccos \left(\frac{bc - a}{\sqrt{1 - b^2}\sqrt{1 - c^2}} \right), \quad B = \arccos \left(\frac{ac - b}{\sqrt{1 - a^2}\sqrt{1 - c^2}} \right), \quad C = \arccos \left(\frac{ab - c}{\sqrt{1 - a^2}\sqrt{1 - b^2}} \right).$$

As it should be, the quantity $\frac{bc-a}{\sqrt{1-b^2}\sqrt{1-c^2}}$ (and its circular permutations as well) in Lemma 5 belongs to $(-1, 1)$. Indeed if $bc \geq a$ then

$$\frac{bc - a}{\sqrt{1 - b^2}\sqrt{1 - c^2}} < 1 \text{ iff } (bc - a)^2 < (1 - b^2)(1 - c^2) \text{ iff } 1 - a^2 - b^2 - c^2 + 2abc > 0.$$

The quantity $1 - a^2 - b^2 - c^2 + 2abc$ is positive because it is the determinant of the covariance matrix (13), which is assumed positive definite. In the case $bc \leq 1$ we would prove similarly that $\frac{bc-a}{\sqrt{1-b^2}\sqrt{1-c^2}} > -1$.

Proof of Lemma 5. The angles are easily computed: if e_1, e_2 and e_3 are the vectors of the canonical basis and L^{-1} is as in (21),

$$\langle L^{-1}e_1, L^{-1}e_2 \rangle = \|L^{-1}e_1\| \cdot \|L^{-1}e_2\| \cdot \cos C, \quad (23)$$

and circular permutations of the above identities hold. The formulas stated in Lemma 5 follow from (23), after having computed the norms and the dot products of the columns of L^{-1} .

An alternative proof is to invert the covariance matrix (13) and to use the orthogonality relations between the angles and their polar angles, see Definition 20. \square

Finally, we stress that the covariance matrix may be interpreted as the Gram matrix

$$\begin{pmatrix} \langle u, u \rangle & \langle u, v \rangle & \langle u, w \rangle \\ \langle u, v \rangle & \langle v, v \rangle & \langle v, w \rangle \\ \langle u, w \rangle & \langle v, w \rangle & \langle w, w \rangle \end{pmatrix},$$

where u, v, w are the three vectors on the sphere which are the columns of the matrix

$$\begin{pmatrix} \frac{\sqrt{1-a^2-b^2-c^2+2abc}}{\sqrt{1-c^2}} & 0 & 0 \\ \frac{\sqrt{bc-a}}{\sqrt{1-c^2}} & -\sqrt{1-c^2} & 0 \\ b & c & 1 \end{pmatrix}.$$

3.4. The reverse construction. Our general construction consists in associating to every model of walk the covariance matrix (13), and thereby a spherical triangle with angles α, β, γ as in Lemma 4. It is natural to ask about the converse: is it possible to realize any spherical triangle as a walk triangle? The answer turns out to be positive, if we allow models of weighted walks.

More specifically, let $\langle x, y, z \rangle$ be an arbitrary spherical triangle, having angles $\alpha, \beta, \gamma \in (0, \pi)$. Introduce $a, b, c \in (-1, 1)$ such that (18) holds. Let finally (U, V, W) be a triplet of independent random variables (actually, having non-correlated variables is enough) with unit variances. Introduce the random variables

$$\begin{pmatrix} Z \\ Y \\ X \end{pmatrix} = L \begin{pmatrix} U \\ V \\ W \end{pmatrix},$$

where L is the matrix (20) appearing in the Cholesky decomposition of the matrix cov. Then by construction the covariance matrix of (X, Y, Z) is (13) and its spherical triangle has angles α, β, γ .

4. ANALYSIS OF HADAMARD MODELS

This section is at the heart of the present paper. We consider Hadamard models in the sense of Section 2.3. Let us briefly recall that these models are characterized by the existence of a decomposition of their inventory (4) as follows:

$$\chi(x, y, z) = U(x) + V(x)T(y, z) \quad \text{or} \quad \chi(x, y, z) = U(x, y) + V(x, y)T(z).$$

As it will be shown in Lemmas 6 and 11, such models admit a quite simple covariance matrix

$$\text{cov} = \begin{pmatrix} 1 & 0 & 0 \\ 0 & 1 & c \\ 0 & c & 1 \end{pmatrix},$$

allowing to perform explicitly many computations. (Notice, however, that the above form for the covariance matrix does not characterize Hadamard models, we construct counterexamples in Section 5.4. These examples lead to the notion of exceptional models.)

In particular, spherical triangles associated to Hadamard models are birectangular, i.e., two (or three) angles are equal to $\frac{\pi}{2}$, see Figure 5. These triangles are remarkable because they are the only ones (with the exception of a few sporadic cases) for which a closed-form expression for the principal eigenvalue does exist. Finally, the exponent (5) of the excursion sequence is computed in Propositions 7 and 12. Using similar techniques as in [18], one can rather easily study the rationality of this exponent.

In the Hadamard (1, 2)-type (Section 4.1), the 2D model associated to $T(y, z)$ dictates the exponent, see Proposition 7. In particular, we prove in Corollary 8 that if the 2D model has a non-rational exponent, then the 3D model is necessarily non-D-finite. To our knowledge, this is the first proof ever of the non-D-finiteness of truly 3D models, making the Hadamard case remarkable. On the other hand, (2, 1)-type Hadamard models (Section 4.2) are more subtle. Their exponents can be computed from exponents of mixtures of two 2D models.

Although we won't do such considerations here, let us emphasize that most of the results in this section hold for weighted walks with arbitrary big jumps: the only crucial point is the existence of a Hadamard decomposition (9) or (10) for the step set.

4.1. (1,2)-Hadamard models.

Lemma 6. *For any (1,2)-type Hadamard model, the matrix cov in (13) takes the particularly simple form*

$$\text{cov} = \begin{pmatrix} 1 & 0 & 0 \\ 0 & 1 & c \\ 0 & c & 1 \end{pmatrix}, \quad \text{with } c = \frac{\frac{\partial^2 T}{\partial y \partial z}}{\sqrt{\frac{\partial^2 T}{\partial y^2} \cdot \frac{\partial^2 T}{\partial z^2}}}(y_0, z_0), \quad (24)$$

where y_0, z_0 are defined in (11). (Notice in particular that c does not depend on the horizontal components U and V in the Hadamard decomposition (9).)

Proof. The proof is elementary. Using the decomposition (9) in the last two equations of the system (11) gives

$$V(x) \frac{\partial T}{\partial y}(y, z) = V(x) \frac{\partial T}{\partial z}(y, z) = 0. \quad (25)$$

As $V(x)$ cannot be equal to 0, we obtain the autonomous system $\frac{\partial T}{\partial y} = \frac{\partial T}{\partial z} = 0$. Let (y_0, z_0) be its unique solution. Moreover, the first equation in (11) leads to

$$U'(x) + V'(x)T(y_0, z_0) = 0$$

which (as $T(y_0, z_0) > 0$) has a unique solution x_0 .

Using once again (9) as well as (25), we deduce that

$$a = V'(x_0) \frac{\partial T}{\partial y}(y_0, z_0) = 0$$

and similarly $b = 0$. The formula (24) for c is a direct consequence of (12) and (9). \square

Our aim now is to compute the spherical angles in the Hadamard case. We could easily use Lemma 4 to deduce Proposition 7 below. Instead we shall do a small detour, which allows us to connect our techniques to the 2D computations performed in [18].

Rather than using the Cholesky decomposition $\text{cov} = LL^\top$, we shall solve $\text{cov} = SS^\top$, with S positive and symmetric. So we need to find the (inverse of the) positive square root

of the covariance matrix, as in Equation (14). According to (24), the covariance matrix has the block structure

$$\text{cov} = \left(\begin{array}{c|cc} 1 & 0 & 0 \\ 0 & & \text{cov}' \\ 0 & & \end{array} \right), \quad \text{with } \text{cov}' = \left(\begin{array}{cc} 1 & c \\ c & 1 \end{array} \right).$$

The inverse of the square root of cov' can be found in [18, p. 52]: $\text{cov}' = S'(S')^\top$, with

$$(S')^{-1} = \frac{1}{2\sqrt{1-c^2}} \left(\begin{array}{cc} \sqrt{1-c} + \sqrt{1+c} & \sqrt{1-c} - \sqrt{1+c} \\ \sqrt{1-c} - \sqrt{1+c} & \sqrt{1-c} + \sqrt{1+c} \end{array} \right).$$

Our conclusion is that

$$S^{-1} = \left(\begin{array}{c|cc} 1 & 0 & 0 \\ 0 & & (S')^{-1} \\ 0 & & \end{array} \right). \quad (26)$$

Proposition 7. *The spherical triangles associated to (1, 2)-type Hadamard models have angles $\frac{\pi}{2}, \frac{\pi}{2}, \arccos(-c)$ (as on Figure 5, left), with c defined in (24). The smallest eigenvalue of the Dirichlet problem λ_1 and the exponent λ are respectively given by*

$$\lambda_1 = \left(\frac{\pi}{\arccos(-c)} + 1 \right) \left(\frac{\pi}{\arccos(-c)} + 2 \right), \quad \lambda = \frac{\pi}{\arccos(-c)} + \frac{5}{2}.$$

Proof. The values of the three angles follow from the formula (26). The expression for λ_1 is a consequence of (17) and finally λ is found in (5). \square

Proposition 7 clearly suggests to compute c and λ , so as to completely characterize the excursion exponent. This happens to be done in [18]: for the 2D unweighted models under consideration, c is always algebraic (possibly rational), and minimal polynomials in the infinite group case are provided in [18, Table 2].

For instance, for the first and second scarecrows on Figure 8 one has $c = -\frac{1}{4}$, while $c = \frac{1}{4}$ for the last scarecrow. Moreover, by [18, Cor. 2], λ is irrational for all infinite group models. This leads to the following corollary:

Corollary 8. *For any (1, 2)-type Hadamard 3D model such that the group associated to the step set T is infinite, the series $O(0, 0, 0; t)$ (and thus also $O(x, y, z; t)$) is non-D-finite.*

We list below important comments on Corollary 8.

- First of all, Corollary 8 is (to the best of our knowledge) the first non-D-finiteness result on truly 3D models. It answers an open question raised in [13, Sec. 9] (concerning the possibility of extending the techniques of [18] to octant models).
- In order to give a concrete application of Corollary 8, consider a model with arbitrary U and V (provided that the model is truly 3D), and with T one scarecrow of Figure 8. This 3D model is non-D-finite since the 2D model associated with T has an infinite group by [21].
- Note that Corollary 8 can be easily extended to models of walks with weights and arbitrary big jumps, provided that the hypothesis on the infiniteness of the group be replaced by the assumption that $\frac{\pi}{\arccos(-c)}$ is non-rational. An algorithmic proof of the irrationality of such quantities is proposed in [18, Sec. 2.4], and further used to some weighted models in [31]. It could certainly be possible to extend it further.

- The proof of Corollary 8 is a direct consequence of [18, Cor. 2], which states that for the 51 unweighted non-singular step sets with infinite group in the quarter plane, the excursion exponent is non-rational. By [18, Thm 3] this implies that the series is non-D-finite.

Remark 9 (Combinatorial interpretation of the exponent). *For (1, 2)-type models, 3D excursions may be decomposed as products of two less-dimensional excursions: a first excursion in the (y, z) -plane with the inventory T and a second 1D excursion in x . This can easily be read on the formula of Proposition 7: writing*

$$\lambda = \left(\frac{\pi}{\arccos(-c)} + 1 \right) + \frac{3}{2},$$

the exponent has a very simple combinatorial interpretation: it is the sum of the exponent of the 2D model (see [18, Thm 4]) and of the universal exponent $\frac{3}{2}$ of a 1D excursion.

Remark 10 (Area of the spherical triangle). *It follows from [9, 18.3.8.4] that the area of the spherical triangle is*

$$\alpha + \beta + \gamma - \pi = \arccos(-a) + \arccos(-b) + \arccos(-c) - \pi \in (0, 2\pi).$$

For birectangular triangles (with say $a = b = 0$) the area becomes $\arccos(-c)$, and is directly related to the smallest eigenvalue (see Proposition 7), as it was the case in 2D.

4.2. (2,1)-Hadamard models.

Lemma 11. *For any (2, 1)-type Hadamard model, the matrix cov in (13) takes the particularly simple form*

$$\text{cov} = \begin{pmatrix} 1 & a & 0 \\ a & 1 & 0 \\ 0 & 0 & 1 \end{pmatrix}, \quad \text{with } a = \frac{\frac{\partial^2 \chi|_{z_0}}{\partial x \partial y}}{\sqrt{\frac{\partial^2 \chi|_{z_0}}{\partial x^2} \cdot \frac{\partial^2 \chi|_{z_0}}{\partial y^2}}}(x_0, y_0), \quad (27)$$

where x_0, y_0, z_0 are defined in (11) and $\chi|_{z_0}(x, y) = \chi(x, y, z_0)$.

Proof. We solve the system (11) in the z -variable first and obtain the point z_0 characterized by $T'(z_0) = 0$. The first two equations of the system (11) read

$$\frac{\partial U}{\partial x}(x, y) + T(z_0) \frac{\partial V}{\partial x}(x, y) = \frac{\partial U}{\partial y}(x, y) + T(z_0) \frac{\partial V}{\partial y}(x, y) = 0.$$

The pair (x_0, y_0) is the critical point associated to the mixture of models (28). \square

Proposition 12. *The spherical triangles associated to (2, 1)-type Hadamard models have angles $\frac{\pi}{2}, \frac{\pi}{2}, \arccos(-a)$ (as on Figure 5, left), with a defined in (27). The smallest eigenvalue of the Dirichlet problem λ_1 and the exponent λ are respectively given by*

$$\lambda_1 = \left(\frac{\pi}{\arccos(-a)} + 1 \right) \left(\frac{\pi}{\arccos(-a)} + 2 \right), \quad \lambda = \frac{\pi}{\arccos(-a)} + \frac{5}{2}.$$

(2,1)-type Hadamard walks and mixing of 2D models. From a probabilistic point of view, the (2, 1)-type is slightly more interesting than the (1, 2)-type. Many computations are indeed related to the concept of mixtures of two 2D probability laws.

More precisely, the polynomials $U(x, y)$ and $V(x, y)$ in (10) both induce a law (or a model) in 2D, which are *mixed* as below:

$$\chi|_{z_0}(x, y) = U(x, y) + T(z_0)V(x, y), \quad (28)$$

the parameter z being specialized at z_0 , the latter being defined by $T'(z_0) = 0$.

In the combinatorial case, for a 3D model we must have $T(z) = z + \bar{z}$, hence $z_0 = 1$ and $T(z_0) = 2$. Equation (28) becomes $U(x, y) + 2V(x, y)$, which is the inventory of a 2D weighted walk (with possible weights 0, 1, 2, 3). Remark that it is not the first appearance of weighted 2D walks in the theory of (unweighted) 3D walks: in [13, Sec. 7] (see in particular Figure 5), 2D projections of 3D models are analyzed, and these projections are typically weighted 2D walks.

Computing a in (27). From a technical point of view, computing a and studying the rationality of $\frac{\pi}{\arccos(-a)}$ requires the same type of computations as above for c and $\frac{\pi}{\arccos(-c)}$ (see Section 4.1). However, some difficulties may occur from the fact that weighted steps are allowed:

- It is not possible to exclude that a model with infinite group has a rational exponent λ (this does not happen in the unweighted case [18], but may happen in the weighted case, see examples in [14]).
- Knowing the critical exponents associated to U and V does not give much information on the exponent of the mixture (28); some evidence is given in Appendix B. The only positive result in that direction is to take step sets with same critical points and covariance matrices. In this case the critical point and the covariance matrix of the mixing remain the same, and explicit computations can be done. For an illustration see Example 14 below.

Applications and examples. We start by a result on non-D-finiteness, for a subclass of $(2, 1)$ -type Hadamard models.

Corollary 13. *For any $(2, 1)$ -type Hadamard 3D model such that the group associated to the step set V is infinite, and $U = V$ or $U = 0$, the series $O(0, 0, 0; t)$ (and thus also $O(x, y, z; t)$) is non-D-finite.*

Corollary 13 applies for several models, but the constraint of taking either $U = V$ or $U = 0$ is quite strong. We now construct a more elaborate example.

Example 14. *Let U, T be any of the first two scarecrows of Figure 8 (possibly the same ones). These models have zero drift (and thus critical point $(0, 0)$) and an easy computation shows that they have the same covariance matrices. Then for any $T(x) = t_1x + t_0 + t_{-1}\bar{x}$, the associated $(2, 1)$ -type Hadamard model defined by (10) is non-D-finite.*

It is the right place to emphasize a link with the article [24], in which the authors develop a theory to (asymptotically) count lattice walks in the quarter plane with inhomogeneities. More precisely, they divide the quadrant in subdomains, say $\mathbb{N}^2 = \bigcup_i D_i$, and to each domain they attach a step set \mathcal{S}_i , which describes the possible moves of the walk when the current position is located at a point of D_i . (The standard homogeneous case is when all \mathcal{S}_i are equal.) It is very difficult to solve such inhomogeneous models in general, but the theory developed in [24] precisely works if the step sets \mathcal{S}_i have same critical points and same covariance matrices (after a proper Cramér transform).

A typical example is to divide the quarter plane as $\mathbb{N}^2 = \mathbb{E} \cup \mathbb{O}$, where \mathbb{E} (resp. \mathbb{O}) is the set of all pairs $(i, j) \in \mathbb{N}^2$ whose sum is even (resp. odd). Theorem 1 in [24] gives an example with this odd-even decomposition in the finite group case; see [24, Thm 4] for the infinite group case (the latter example also uses scarecrow models of Figure 8).

4.3. Hadamard product of generating functions. In this section, which is essentially borrowed from [13], we explain that for models admitting a Hadamard decomposition, the generating function $O(x, y, z; t)$ in (1) is a Hadamard product of two less-dimensional

(coloured) counting problems, see (29) below. Although this discussion may be extended to an arbitrary dimension, we focus here on the dimension three.

In order to have a uniform presentation of the $(1, 2)$ - and $(2, 1)$ -types, we temporary rename the variables x, y, z in x_1, x_2, x_3 . Moreover, we denote the d -tuple $(0, \dots, 0)$ by 0^d . Assume there exist $d \in \{1, 2\}$ and three sets $\mathcal{U} \in \{-1, 0, 1\}^d \setminus \{0^d\}$, $\mathcal{V} \in \{-1, 0, 1\}^d$ and $\mathcal{T} \in \{-1, 0, 1\}^{3-d} \setminus \{0^{3-d}\}$. Then the model is said to be $(d, 3-d)$ -Hadamard if the step set \mathcal{S} admits the decomposition (or factorization)

$$\mathcal{S} = (\mathcal{U} \times \{0^{3-d}\}) \cup (\mathcal{V} \times \mathcal{T}).$$

Let \mathcal{C}_1 be the set of walks with steps in $\mathcal{U} \cup \mathcal{V}$ confined to \mathbb{N}^d , in which the steps are coloured black and white, with the condition that all steps of $\mathcal{U} \setminus \mathcal{V}$ are white and all steps of $\mathcal{V} \cup \mathcal{U}$ are black. Let $C_1(x_1, \dots, x_d, v; t)$ be the associated generating function, where t keeps track of the length, x_1, \dots, x_d of the coordinates of the endpoint, and v of the number of black steps. Let $C_2(x_{d+1}, x_3; v)$ be the generating function of \mathcal{T} -walks confined to \mathbb{N}^{3-d} , counted by the length v and the coordinates of the endpoint (x_{d+1}, x_3) . Then Proposition 5.1 of [13] says that

$$O(x_1, x_2, x_3; t) = C_1(x_1, x_d, v; t) \odot_v C_2(x_{d+1}, x_3; v)|_{v=1}, \quad (29)$$

where \odot_v denotes the Hadamard product with respect to v :

$$\sum_i a_i v^i \odot_v \sum_j b_j v^j = \sum_i a_i b_i v^i,$$

the resulting series in (29) being specialized to $v = 1$.

In the $(1, 2)$ -type, \mathcal{U} and \mathcal{V} are of dimension one, and thus C_1 is algebraic, hence D-finite, as it corresponds to a 1D (coloured) counting problem. So if the generating function C_2 associated to \mathcal{T} is D-finite, then $O(x_1, x_2, x_3; t)$ will remain D-finite, since the Hadamard product preserves D-finiteness [52]. A similar remark applies to the $(2, 1)$ -type.

On the other hand, there is no systematic result saying that taking the Hadamard product of a D-finite function by a non-D-finite function leads to a non-D-finite function. However we do think that such a result should hold in our case: this would mean to prove Corollaries 8 and 13 directly, at the level of generating functions, using for instance singularity analysis.

5. CLASSIFICATION OF THE MODELS AND EIGENVALUES

5.1. Motivations and presentation of the results. In this section we would like to classify the 11,074,225 models with respect to their triangle and the associated principal eigenvalue. The central idea is that there is a strong link between the group (as defined in Section 2.2) and the triangle. To understand this connection, we propose a novel geometric interpretation of the group, as a reflection group on the sphere; this interpretation is very natural and manipulable. More precisely we will interpret the three generators of the group as the three reflections with respect to the sides of the spherical triangle. We shall present three main features:

- *Finite group case* (Section 5.2): we interpret the group G as a tiling group of the sphere, see Table 3, as well as Figures 6 and 11. We also explain a few remarkable facts observed in the tables of [2], on the number of different asymptotic behaviors observed.
- *Infinite group case* (Section 5.3): typically the existence of a relation between the generators of the group can be read off on the angles. The simplest example is

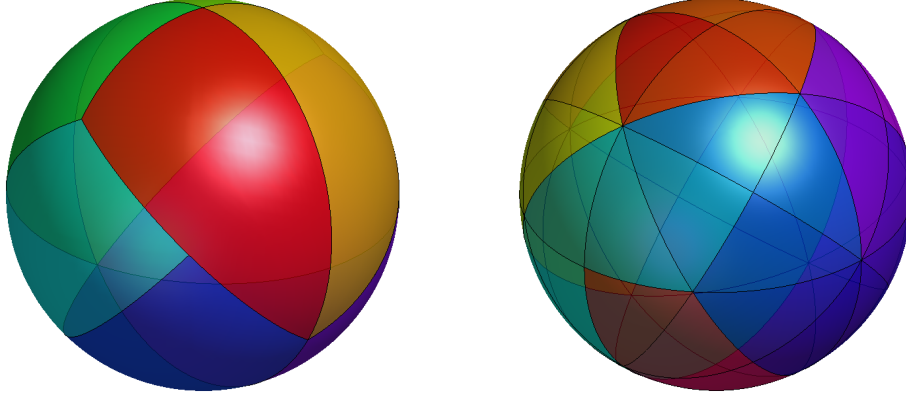


FIGURE 11. Tilings associated to the triangles with angles $\frac{\pi}{3}, \frac{\pi}{2}, \frac{2\pi}{3}$ (left) and $\frac{\pi}{4}, \frac{\pi}{3}, \frac{\pi}{2}$ (right). These triangles correspond to the lines 9 and 17 on Table 3

the relation $(ab)^m = 1$, which on the triangle will correspond to an angle equal to $k\pi/m$ for some integer k . In particular, all triangles from the group

$$G_3 = \langle a, b, c \mid a^2, b^2, c^2, (ac)^2, (ab)^2 \rangle$$

of Table 1 (the Hadamard models) will have two right angles.

- *Exceptional models* (Section 5.4): for some infinite group models (a few hundreds of thousands), some unexpected further identities on the angles hold—*unexpected* means not implied by a relation between the generators, as explained above.

The most interesting case is given by 28 893 models in G_1 and 1 552 in G_2 , which have a triangle with exactly 2 right angles. Although these models do not have a Hadamard structure, their triangle has the same type as classical Hadamard models, and the principal eigenvalue (and hence the critical exponent) can be computed in a closed form.

There are also some models with infinite group but three right angles (in this case, the exponent is $\frac{9}{2}$, and cannot be used to detect non-D-finiteness). Let us finally mention two models with infinite group and having the same triangle as Kreweras 3D. See Theorem 17 for a more precise and complete statement.

To summarize, classifying the triangles is close, but different, to classifying the groups. The latter task has already been achieved in [2] (finite group case; we have reproduced their results in Table 4) and [48] (infinite groups; see our Table 1), using a heavy computer machinery. However, the group classification is more precise, in the sense that the spherical triangle does not determine everything: infinite group models can have a tiling triangle, and the Hadamard models are not the only ones to have birectangular triangles.

5.2. Finite group case.

Some aspects of the group. Let us recall from Section 2.2 that it is possible to attach to any small step octant model a group $G = \langle \phi, \psi, \tau \rangle$ of involutions (i.e., $\phi^2 = \psi^2 = \tau^2 = 1$). The analytic expression of the generators ϕ, ψ and τ is given in (8), it uses the coefficients of the inventory χ .

This group was first introduced in the context of 2D walks [35, 21] and turns out to be very useful; let us recall a few applications of this concept:

- When the group is finite and if in addition the orbit-sum of the monomial $x_1 \times \cdots \times x_d$ under the group G , namely

$$\text{OS}(x_1, \dots, x_d) = \sum_{g \in G} \text{sign}(g) \cdot g(x_1 \times \cdots \times x_d), \quad (30)$$

is non-zero, one may obtain closed-form expressions for the generating function. See [21] for the initial application of this technique, called the orbit-sum method; it was further used in [49, 14].

- When the group is finite but the orbit-sum (30) is zero, it is still possible, in a restricted number of cases, to derive an expression for the generating function, see [21, 49, 14] for examples. The applicability of this technique is not completely clear.
- Last but not least, in dimension 2 there is equivalence between the finiteness of the group and the D-finiteness of the generating functions (this is a consequence of the papers [21, 16, 50] altogether).

Let us now examine each of the above applications in dimension 3. The first item is still valid, as shown in [13, 58]. As in the 2D case, the second item only works for a few cases. For instance, Figure 4 in [13] gives a list of 19 non-Hadamard 3D models with finite group and zero orbit-sum, which are not solved at the moment. Finally, the third item is an open question (in our opinion very exciting!). As an illustration, all 19 previous models (including Kreweras 3D model) have a finite group, but as explained in [13, Sec. 6.2], these models do not seem D-finite. In this case, the equivalence in the third item would not be satisfied.

Connection between combinatorial and geometric aspects. We have numerically computed the critical exponents for each one of the models corresponding to a finite group, using the fundamental eigenvalue of the associated spherical triangles. The computation procedure is described in Section 6. Our results are summarized in Table 3.

It is remarkable that among all possible 17 exponents, each one is uniquely assigned to a particular spherical triangle. Moreover, each group can be realized as a reflection group for the associated triangles, giving a nice connection between combinatorial and geometric aspects. More precisely, we notice that all triangles associated to models with finite groups are *Schwarz triangles*, which means that they can be used to tile the sphere, possibly overlapping, through reflection in their edges. They were classified in [55] and a nice theoretical and graphical description can be seen on the associated Wikipedia page (see the [ur1](#)). The classification of Schwarz triangles also includes information about their symmetry groups, which are seen to coincide with the combinatorial groups.

We recall that when the associated spherical triangle has two right angles, then explicit formulas exist for the first eigenvalue. Therefore values of the eigenvalue and exponent given in Table 3 which are written as rational numbers are exact. For the other values, numerical approximation was used in the computation of the eigenvalue and the exponent (see Section 6 for the details). We believe that all digits shown are accurate.

Some remarks on the tables of [2]. In this paragraph we recall a few conjectural comments which appear in the captions of Tables 2, 3 and 4 of [2], that we can explain using the spherical triangles.

First, Table 2 of [2] gives the guessed asymptotic behavior of the 12 models with group $\mathbb{Z}_2 \times S_4$ and zero orbit-sum (see our Table 4). The first remark of [2] is that the critical

	Eigenvalue	Exponent	Nb tri.	Angles	Hadamard	Gr. Size	Group
1	4.261735	3.124084	2	$\frac{2\pi}{3}, \frac{3\pi}{4}, \frac{3\pi}{4}$	no	48	$\mathbb{Z}_2 \times S_4$
2	5.159146	3.325757	7	$\frac{2\pi}{3}, \frac{2\pi}{3}, \frac{2\pi}{3}$	no	24	S_4
3	6.241748	3.547890	2	$\frac{\pi}{2}, \frac{2\pi}{3}, \frac{3\pi}{4}$	no	48	$\mathbb{Z}_2 \times S_4$
4	6.777108	3.650869	5	$\frac{\pi}{2}, \frac{2\pi}{3}, \frac{2\pi}{3}$	no	24	S_4
5	70/9	23/6	41	$\frac{\pi}{2}, \frac{\pi}{2}, \frac{3\pi}{4}$	yes	16	$\mathbb{Z}_2 \times D_8$
6	35/4	4	279	$\frac{\pi}{2}, \frac{\pi}{2}, \frac{2\pi}{3}$	yes/no	12	D_{12}
7	12	9/2	1852	$\frac{\pi}{2}, \frac{\pi}{2}, \frac{\pi}{2}$	yes	8	$\mathbb{Z}_2 \times \mathbb{Z}_2 \times \mathbb{Z}_2$
8	12.400051	4.556691	2	$\frac{\pi}{3}, \frac{\pi}{2}, \frac{3\pi}{4}$	no	48	$\mathbb{Z}_2 \times S_4$
9	13.74435	4.740902	7	$\frac{\pi}{3}, \frac{\pi}{2}, \frac{2\pi}{3}$	no	24	S_4
10	20	11/2	172	$\frac{\pi}{3}, \frac{\pi}{2}, \frac{\pi}{2}$	yes/no	12	D_{12}
11	20.571964	5.563109	2	$\frac{\pi}{4}, \frac{\pi}{2}, \frac{2\pi}{3}$	no	48	$\mathbb{Z}_2 \times S_4$
12	21.309407	5.643211	7	$\frac{\pi}{3}, \frac{\pi}{3}, \frac{2\pi}{3}$	no	24	S_4
13	24.456910	5.970604	2	$\frac{\pi}{4}, \frac{\pi}{3}, \frac{3\pi}{4}$	no	48	$\mathbb{Z}_2 \times S_4$
14	30	13/2	41	$\frac{\pi}{4}, \frac{\pi}{2}, \frac{\pi}{2}$	yes	16	$\mathbb{Z}_2 \times D_8$
15	42	15/2	5	$\frac{\pi}{3}, \frac{\pi}{3}, \frac{\pi}{2}$	no	24	S_4
16	49.109942	8.025663	2	$\frac{\pi}{4}, \frac{\pi}{4}, \frac{2\pi}{3}$	no	48	$\mathbb{Z}_2 \times S_4$
17	90	21/2	2	$\frac{\pi}{4}, \frac{\pi}{3}, \frac{\pi}{2}$	no	48	$\mathbb{Z}_2 \times S_4$

TABLE 3. Characterization of triangles and exponents associated to models with finite groups. One can see some eigenvalues appearing in Lemma 25

Group	Hadamard	Non-Hadamard OS $\neq 0$	Non-Hadamard OS = 0
$\mathbb{Z}_2 \times \mathbb{Z}_2 \times \mathbb{Z}_2$	1852	0	0
D_{12}	253	66	132
$\mathbb{Z}_2 \times D_8$	82	0	0
S_4	0	5	26
$\mathbb{Z}_2 \times S_4$	0	2	12

TABLE 4. Number of models with finite group. Note that OS refers to the orbit-sum defined in (30). The original version of this table may be found in [2, Table 1]

exponent β of the generating function $O(1, 1, 1; t)$ seems to be related to the excursion exponent λ by the formula

$$\beta = \frac{\lambda}{2} - \frac{3}{4}. \quad (31)$$

(Notice that the remark in [2] is stated with $+\frac{3}{4}$ and not $-\frac{3}{4}$; the reason is that our critical exponents are the opposite of the ones in [2].) Let us briefly mention that (31) is indeed true and is a consequence of Denisov and Wachtel results [29]: by (5) (resp. [29, Thm 1]) one has

$$\lambda = \sqrt{\lambda_1 + \frac{1}{4}} + 1 \quad \text{and} \quad \beta = \frac{1}{2} \left(\sqrt{\lambda_1 + \frac{1}{4}} - \frac{1}{2} \right), \quad (32)$$

for zero-drift models (which is the case of these models under consideration). This remark also applies to [2, Table 3], giving the excursion asymptotics for the 26 models whose group is S_4 and orbit-sum zero (see again our Table 4).

The second comment of [2] that we can easily explain is about the number of different critical exponents. It is remarked in [2] that each exponent λ seems to appear for exactly two models in their Table 2, and that in their Table 3 there are only four different exponents (namely, -5.64321 , -4.74090 , -3.65086 and -3.32575). This simply follows from the fact that in [2, Table 2] (resp. [2, Table 3]) there are only six (resp. four) types of spherical triangles, which appear twice for the second table.

Remark 15 (Second Kreweras eigenvalue). *The triangle on the ninth line of Table 3 is exactly the half of Kreweras triangle. Accordingly (and this was confirmed by our numerical approximations) the principal eigenvalue of the models with half Kreweras triangle equals the second smallest eigenvalue of Kreweras model.*

5.3. Infinite group case. We have numerically computed for each model corresponding to an infinite group its associated spherical triangle, the eigenvalue and thus, the exponent. Details about numerical computations can be found in Section 6.

As expected, the behavior is irregular (much more than in the finite group case) and the number of distinct eigenvalues, leading to distinct exponents, is more important. Therefore, we do not attempt to classify the models by the associated eigenvalues. In order to illustrate their repartition, we show in Figure 12 the distribution of the eigenvalues for triangles in associated to the models in G_1 , G_2 and G_3 found in Table 1. The points having the y -coordinate zero represent the cases where the steps of the model belong to the same half-space.

As in the finite group case, we wonder if there is a connection between the triangles associated to the models and their associated combinatorial group. We believe that the analogue proposition holds also for the infinite groups: the combinatorial groups can be realized as groups of symmetries for the associated triangle, taking as generators the three elementary reflections or combinations of them as indicated in the analysis in [48]. In some cases, like for example when the triangle has two angles equal to $\pi/2$, the realization of the infinite group as a symmetry group for the triangle is more evident.

Analyzing our computations we find that the following result holds.

Theorem 16. *All triangles associated to non-degenerate models with infinite groups satisfy the following property: the combinatorial group can be realized as a symmetry group of the triangle. We have two possibilities:*

- *The generators a, b, c are the reflections with respect to the three sides of the triangle.*

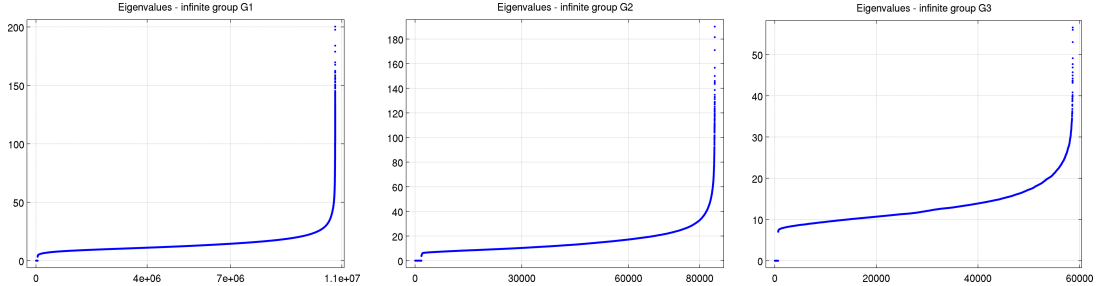


FIGURE 12. Distribution of eigenvalues for triangles associated to the infinite groups G_1 , G_2 and G_3 from Table 1

- In cases where the first possibility does not hold, it suffices to replace one of the reflections by its conjugate with respect to one of the other two (for example replace \mathbf{a} by \mathbf{bab}). Note that this corresponds nicely with arguments shown in [48].

Our proof of Theorem 16 relies on the numerical computations made using the tools from Section 6. We note that only information on the angles of the triangles is needed here, which can be obtained using elementary functions and algebraic numbers. Therefore the arguments below can be justified using symbolic computations.

Proof. For G_1 there is nothing to prove: we may choose $\mathbf{a}, \mathbf{b}, \mathbf{c}$ to be the three reflections with respect to the sides of the triangle, and no additional relation is required.

Among the 82 453 triangles associated to non-degenerate models of type G_2 , exactly 79 219 have (at least) one right angle. Therefore, if \mathbf{a}, \mathbf{b} are reflections with respect to the sides adjacent to the right angle, then $(\mathbf{ab})^2 = 1$. The remaining 3 234 triangles have the property that for one particular labeling $\mathbf{a}, \mathbf{b}, \mathbf{c}$ of the symmetries associated to the sides of the triangles, the composition \mathbf{cacb} is a rotation of angle π and therefore $(\mathbf{cacb})^2 = 1$. Therefore, after the transformation of the type $\mathbf{a} \leftarrow \mathbf{cac}$ described in [48], G_2 is represented as a group of symmetries of the associated triangles.

All triangles associated to non-degenerate models in G_3 have at least two angles equal to $\pi/2$, and 40 among these have (surprisingly) three right angles. Therefore, there is a labeling $\mathbf{a}, \mathbf{b}, \mathbf{c}$ of the reflections with respect to the sides of the triangles for which $(\mathbf{ab})^2 = 1$ and $(\mathbf{ac})^2 = 1$.

For triangles associated to groups among G_4, \dots, G_{11} (all models in G_{12} are included in a half-space) the relations are not always immediately identifiable with geometric aspects related to angles. One may find triangles with angles π/k for groups having relations of the type $(\mathbf{ab})^k = 1$, but this is not always the case. In order to validate these cases we used the following procedure:

- (i) For a triangle T associated to a group G_n , $n = 4, \dots, 11$, for every one of the six permutations of the reflections $\mathbf{a}, \mathbf{b}, \mathbf{c}$, we construct the result of the transformations $\mathcal{R}(\mathbf{a}, \mathbf{b}, \mathbf{c})(T)$, where \mathcal{R} varies among the relations of the group G_n . We test if the resulting triangle after the above transformations coincides with the initial triangle. If this is the case for every relation \mathcal{R} of G_n then we have found a representation of G_n as a group of reflections.
- (ii) If the above step fails, then we consider transformations of the type $\mathcal{R}(\mathbf{cac}, \mathbf{b}, \mathbf{c})$ where, as before, $\mathbf{a}, \mathbf{b}, \mathbf{c}$ are reflections along the sides of the triangles and \mathcal{R} varies among the relations of G_n .

For $G_5, G_7, G_8, G_9, G_{10}, G_{11}$ the step (i) of the above procedure finds a permutations of basic symmetries which satisfies the group relations. This also works partially for G_4 and G_6 . For all the remaining cases, the step (ii) finds a combination of reflections with one modification of the type $\mathbf{a} \leftarrow \mathbf{cac}$ such that G_n is represented again as a symmetry group of the triangle. \square

5.4. Exceptional models. Let us start by recalling that the typical situation is that relations between generators of the group have strong consequences on the angles of the triangle. For example, a relation of the type $(\mathbf{ab})^2 = 1$ gives, in most cases, that the triangle has one right angle.

In this section we are interested in a family of models, which is remarkable in the sense that the triangle has additional symmetries than those implied by the relations between the generators. We identify models which are non-Hadamard and which have two right angles, providing additional examples where we may compute exponents explicitly. Moreover, we identify triangles associated to infinite groups with three right angles or three angles equal to $2\pi/3$.

Theorem 17. *Among all infinite group 3D models,*

- 200 models in G_6 , 837 in G_4 , 77 667 in G_2 and 31 005 in G_1 have exactly one right angle;
- 57 935 models in G_3 , 1 552 in G_2 and 28 893 in G_1 have exactly two right angles;
- 40 models in G_3 and 563 models in G_1 have three right angles (see Figure 13 for two examples);
- 2 models in G_4 and 3 models in G_1 have three $2\pi/3$ angles (see Figure 13).

Lists with steps corresponding to each one of the cases presented in the above result can be accessed at the following link: <https://bit.ly/2J4Vf3X>.

Remark 18 (On the statement and the proof of Theorem 17). *The part of Theorem 17 which is really a theorem is the existence of models having remarkable angles as described in the statement. On the other hand, we have used numerical tools to find the numbers of models in each category (e.g., 200 models in G_6 having exactly one right angle): we inspect the triangles by using methods described in Section 6 and use a tolerance of 10^{-8} in order to classify the angles of the triangle.*



FIGURE 13. Left: two models with a group G_3 and three right angles. Right: two friends of Kreweras 3D, i.e., models from G_4 with three angles of measure $2\pi/3$

The first consequence of Theorem 17 is to illustrate that the spherical triangle does not determine everything:

- infinite group models can have triangles which tile the sphere,
- Hadamard models are not the only ones to admit birectangular triangles.

Note that the first phenomenon already appears in 2D: it is indeed possible to construct two-dimensional models with infinite group and rational exponent, see, e.g., [14]. All known examples have either small steps and weights (not only 0 and 1), or admit at least one big jump. However, restricted to the unweighted case there is equivalence between the

infiniteness of the group and the irrationality of the exponent [18]. This miracle in 2D is due to the fact that there are only 51 (non-singular) infinite group models—and more than 11 millions 3D models.

The second consequence of Theorem 17 is the following:

Corollary 19. *For any of the 57 935 models in G_3 , 1 552 in G_2 and 28 893 in G_1 which have exactly two right angles (say $a = b = 0$), the exponent is given by*

$$\lambda = \frac{\pi}{\arccos(-c)} + \frac{5}{2}.$$

In particular if $\frac{\pi}{\arccos(-c)} \notin \mathbb{Q}$ then the model is non-D-finite.

As an example of Corollary 19, we prove that the two models of Figure 14 admit non-rational exponents. We present an alternative approach to the irrationality proof given in [18, Sec. 2.4], which goes much further to the two examples of 14.

Proof. Assume that $\arccos(-c) = \frac{p}{q}\pi$. Then obviously $\cos(q \arccos(-c)) - (-1)^p = 0$, and thus c is a root of

$$f(x) = \cos(q \arccos(-x)) - (-1)^p, \quad (33)$$

which is (up to an additive constant) a Chebychev polynomial. For the first (resp. second) model on Figure 14, one has $c = \sqrt{7}/3$ (resp. $\sqrt{7/10}$), having respective minimal polynomials

$$P(X) = 9X^2 - 7 \quad \text{and} \quad P(X) = 10X^2 - 7. \quad (34)$$

Since Chebychev polynomials have leading coefficient one or a power of 2, this is the same for $f(x)$.

We recall that a polynomial in $\mathbb{Z}[X]$ is called *primitive* if its coefficients have no common factor. Gauss' lemma is a well known result in number theory which states that the product of two primitive polynomials is again primitive.

Suppose that P is a primitive polynomial and that P divides, in $\mathbb{Q}[X]$, the polynomial f defined in (33). Then there exists another polynomial $Q \in \mathbb{Q}[X]$ such that $f = PQ$. Suppose that Q does not have integer coefficients. Then, let c_Q be the least common multiple of the denominators of the coefficients of Q . In this way, the polynomial $c_Q Q$ has integer coefficients and is primitive. Therefore

$$P \cdot (c_Q Q) = c_Q f,$$

and since P and $c_Q Q$ are both primitive, it follows by Gauss' lemma above that $c_Q f$ is also primitive. This leads to a contradiction if $c_Q > 1$. Therefore $Q \in \mathbb{Z}[X]$.

We can now finish the proof and give the following general result: if $P \in \mathbb{Z}[X]$ is a primitive polynomial and the leading coefficient of P is greater than 2 and is not a power of 2, then P cannot divide f . Using the argument given in the previous paragraph we can conclude that f admits a decomposition of the type $f = PQ$ with $Q \in \mathbb{Z}[X]$. Therefore the leading coefficient of f is a product of the leading coefficients of P and Q . Since the leading coefficient of P is greater than 2 and is not a power of 2, it cannot divide the leading coefficient of f , which is a power of 2.

In particular, both polynomials in (34) are primitive and have leading coefficient greater than 2, but not a power of 2. Therefore they cannot divide f , and as a consequence the exponent cannot be rational in these cases. \square



FIGURE 14. Two models having a group G_2 (Table 1). Despite these models do not have the Hadamard structure, they admit birectangular triangles and thus explicit eigenvalues, providing examples of application to Corollary 19

5.5. Equilateral triangles. Contrary to the usual planar geometry, there exists in spherical geometry a one-parameter family of equilateral triangles: for any $\alpha \in (\pi/3, \pi)$ there exists an equilateral triangle with angles equal to α . The limit case $\alpha = \pi/3$ (resp. $\alpha = \pi$) is the empty triangle (resp. the half-sphere).

Among the 11 millions of models, we have found 279 different equilateral triangles. The most remarkable ones admit the angles $\pi/2$ (the simple walk), $2\pi/3$ (Kreweras), $\arccos(1/3)$ (polar triangle for Kreweras), $\arccos(\sqrt{2}-1)$ (the smallest equilateral triangle), $2\pi/5$, $3\pi/5$. It seems that only the first one admits an eigenvalue in closed-form.

Except for the equilateral triangles with angles $\pi/2$ and $2\pi/3$, which exist in G_3 and G_4 , all other equilateral triangles come from G_1 . The list of equilateral triangles in G_1 and the list of all possible angles observed can be consulted on the webpage of the article: <https://bit.ly/2J4Vf3X>.

6. NUMERICAL APPROXIMATION OF THE CRITICAL EXPONENT

6.1. Literature. In lattice walk problems (and more generally in various enumerative combinatorics problems), it is rather standard to generate many terms of a series (as many as possible), and to try to predict the behavior of the model, as the algebraicity or D-finiteness of the generating function, or the asymptotic behavior of the sequence. Having a large number of terms allows further to derive estimates of the exponential growth or of the critical exponent. More specifically, in the context of walks confined to cones, it is possible to make use of a functional equation to generate typically a few thousands of terms (the functional equation corresponds to a step-by-step construction of a walk, see [13, Eq. (4.1)] for a precise statement).

In particular, one can find in [15, 2, 42] various estimates of critical exponents (note that contrary to the results presented here, the estimates of [15, 2, 42] also concern the total numbers of walks—and not only the numbers of excursions). In [15], Bostan and Kauers consider 3D step sets of up to five elements, and guess various asymptotic behaviors using convergence acceleration techniques. Bacher, Kauers and Yatchak go further in [2], computing more terms and considering all 3D models (with no restriction on the cardinality of the step set). In [42], Guttmann analyses the coefficients of a few models by either the method of differential approximants or the ratio method. The methods of [42] for generating the coefficients and for analyzing the resulting series are given in Chapters 7 and 8 of the book [41].

Our techniques are completely different here: we develop a finite element method and compute precise approximations of the eigenvalue (typically, 10 digits of precision). This method can be applied to any spherical triangle, independently of the fact that it corresponds, or not, to a random walk model. We make available our codes at the following link: <https://bit.ly/2J4Vf3X>.

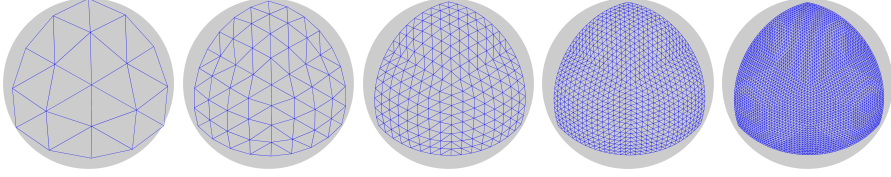


FIGURE 15. Triangulation of a spherical triangle using successive refinements

6.2. Finite element method. As already stated before in the paper, the results of [28, 6, 29] allow to compute the exponent with the aid of the first eigenvalue of the Laplace-Beltrami operator for a region of the unit sphere. In the cases studied here, this amounts to finding the first eigenvalue of a spherical triangle. Various methods were employed in the literature, especially for finding the first eigenvalue of the triangle corresponding to the tetrahedral partition. We mention [53, 54, 11]. A method for computing eigenvalues of spherical regions using fundamental solutions was recently proposed in [1] for smooth domains on the sphere. The singular behavior generated by the corners of the triangles makes that this method is not directly adapted to our needs. In the following we use the finite element method to compute the eigenvalues of spherical triangles. The finite element computation consists in a few standard steps. For general aspects regarding finite element spaces defined on surfaces, we refer to [34]. We underline the fact that the method described below can be applied to general subsets of the sphere, not only for triangles.

(a) Triangulation of the domain. In order to discretize the spherical triangle, we consider triangulations. For simplicity, we work with triangulations with flat triangles, which approximate the curved surface of the sphere better and better as the number of triangles increases. In order to construct such triangulations, we use the classical midpoint refinement procedure. Starting from a triangle, we construct the midpoints projected on the sphere, and we replace the initial triangle with four smaller triangles. We iterate this procedure a few times until we reach the desired precision. The triangulation procedure is described in Algorithm 1. Details concerning the number of refinements and the precision will be discussed below. An illustration of the triangulation procedure can be seen in Figure 15.

Algorithm 1 Constructing a triangulation of a spherical triangle

Require:

- L : Three distinct points A, B, C on the sphere.
- k : number of refinements

- 1: Initialize the set of vertices \mathcal{P}
- 2: Initialize the set of triangles \mathcal{T}
- 3: **for** $iter = 1 : k$ **do**
- 4: **for** $T_i = XYZ \in \mathcal{T}$ **do**
- 5: Construct M_1, M_2, M_3 the projections on the sphere of the midpoints of T_i ;
- 6: Add M_1, M_2, M_3 to \mathcal{P}
- 7: Remove T_i from \mathcal{T}
- 8: Add the four triangles determined by X, Y, Z, M_1, M_2, M_3 to \mathcal{T}
- 9: **end for**
- 10: **end for**

return \mathcal{P}, \mathcal{T}

(b) Assembly. Given a triangulation of the spherical triangle \mathcal{T} we denote by $(n_j)_{j=1}^N$ an enumeration of the nodes and by $(T_i)_{i=1}^M$ an enumeration of the triangles. Each T_i contains the associated nodes to its three vertices. On the triangulation \mathcal{T} we consider the $P1$ -Lagrange finite element space. This consists of associating to each node n_j in the discretization a finite element function φ_j which is piecewise affine on each of the triangles T_i such that $\varphi_j(n_k) = \delta_{ik}$. A function $u \in H^1(\mathcal{T})$ is approximated by a linear combination of the finite element functions

$$u \approx \sum_{j=1}^N a_j \varphi_j.$$

A standard approach in numerical computations is to use the weak formulation of the Laplace-Beltrami eigenvalue problem

$$\int_{\mathcal{T}} \nabla_{\tau} u \cdot \nabla_{\tau} v = \lambda \int_{\mathcal{T}} u v, \quad \forall v \in H^1(\mathcal{T}),$$

where ∇_{τ} represents the tangential gradient to the surface of the sphere. When replacing u and v by their finite element approximations $u \approx \sum_{j=1}^N a_j \varphi_j$ and $v \approx \sum_{j=1}^N b_j \varphi_j$, we obtain the discrete version

$$\mathbf{v}^t K \mathbf{u} = \lambda \mathbf{v}^t M \mathbf{u}, \quad \forall \mathbf{v} \in \mathbb{R}^N, \quad (35)$$

where $\mathbf{u} = (a_1, \dots, a_N)$ and $\mathbf{v} = (b_1, \dots, b_N)$. Here we have denoted with K the rigidity matrix and with M the mass matrix:

$$K = \left(\int_{\mathcal{T}} \nabla_{\tau} \varphi_i \cdot \nabla_{\tau} \varphi_j \right)_{1 \leq i, j \leq n}$$

$$M = \left(\int_{\mathcal{T}} \varphi_i \varphi_j \right)_{1 \leq i, j \leq n}$$

The matrices K and M are computed explicit for every triangulation.

(c) Solving the discretized problem. We notice that the problem (35) is equivalent to the generalized eigenvalue problem

$$K \mathbf{u} = \lambda M \mathbf{u}.$$

We are interested in the smallest eigenvalue associated to this problem. We solve this problem using the `eigs` function in Matlab.

6.3. Improving the precision using extrapolation. We start by testing our algorithm for the spherical triangle having three right angles, for which the first eigenvalue is known and is equal to 12. After 11 refinements we arrive at the value 12.000 001 608 by using 12 589 057 discretization points. This is at the limit of what we can do using the finite element method without parallelization. The computation took 12 minutes and used over 80GB of RAM memory.

It is possible to improve the precision by using some extrapolation procedures. Various techniques for improving the convergence of a sequence based on a finite number of terms can be found in [12]. We choose to use Wynn's epsilon algorithm, which starting from $2n+1$ terms can deliver the exact limit of a sequence, whenever this sequence can be written as a sum of n geometric sequences. For any discretization parameter h small enough the discrete eigenvalue approximation λ_h has a Taylor-like expansion

$$\lambda_h = \lambda + C_1 h^{k_1} + C_2 h^{k_2} + \dots$$

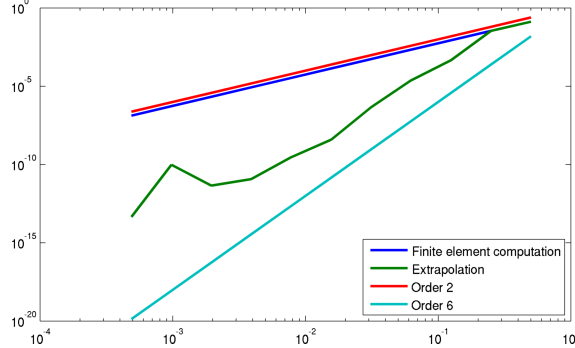


FIGURE 16. Improvement of the convergence rate when applying the extrapolation procedure using Wynn's epsilon algorithm

where k_i is an increasing sequence of positive real numbers. Applying Wynn's epsilon algorithm to a sequence of approximation corresponding to $h, h/2, \dots, h/2^k$ will cancel the first terms in the above expansion, giving a better convergence rate. Applying the extrapolation procedure for the triple right angle triangle recalled above with 11 refinement steps gives us the value 11.999 999 999 999 46 which is close to machine precision.

Wynn's epsilon algorithm is described in [12, p. 247]. An illustration of the improvement of the convergence rate in the case of the triple right angle triangle is given in Figure 16. One may note that the initial finite element approximation has convergence of order 2, which is to be expected (see [38, 45]). On the other hand, the extrapolation procedure seems to have order of convergence at least 6, quickly reaching close to machine precision. Examples of applications of Wynn's algorithm and other extrapolation procedures can be found in [12], together with Matlab codes.

6.4. Computing exponents. When given a sequence of steps corresponding to a 3D walk, the first step is to test if all points belong to the same half-space, determined by a plane passing through the origin (see our assumption (H)). We choose to loop over all pairs of steps and test if all the remaining points are on the same side of the plane determined by the current pair and the origin.

Once we confirm that the current sequence of steps is not contained in a half-space, we know that the inventory χ has a unique minimum point (which is obviously a critical point) in the positive octant. We use a numerical optimization procedure in order to find this minimizer. It is straightforward to compute the gradient and the Hessian of the inventory χ , therefore a Newton algorithm is applicable. We use the function `fmincon` from the Matlab Optimization Toolbox to find the minimizers. In all our computations the numerical solution satisfies the critical equations (11) with a numerical precision between 10^{-16} and 10^{-12} . We mention that for cases of interest, exact solutions can be found (using Maple, for example; see [18, Sec. 2.4]). We choose to work with numerical approximations in view of the large number of computations involved in our study.

Once the critical point is found, we may compute the coefficients a, b, c of the covariance matrix and find the associated spherical triangle like described in Theorem 2. Next we apply the procedure described in Sections 6.2 and 6.3 in order to compute the eigenvalue of the triangle. The exponent is then computed using the formula (5).

We make available our codes for constructing the triangulation, matrix assembly, eigenvalue computation and extrapolation procedure. You can access them at the following link: <https://bit.ly/2J4Vf3X>.

6.5. Discussion of the computations. We underline that the computation of the critical points of the inventory function can be computed using symbolic computations. This means that the angles of the triangles can be computed exactly in terms of algebraic numbers and elementary functions. We have a Matlab code which can do this for the majority of the cases we tested and it can be consulted on the webpage associated to this article.

Since the number of models involved in this study is very large (over 11 millions), we choose to perform our computations in Matlab using floating point arithmetic (16 significant digits of precision). This leads to a significant acceleration of the computations. The computation of the eigenvalues is done using 7 refinement steps for finite groups (typically 8 digits of precision) and 5 refinement steps for the infinite groups (6 digits of precision).

Computations for the models associated to finite groups took a few hours on a laptop with an i7 processor and 16GB of RAM memory. Computations for the infinite groups G_2, G_3, \dots, G_{12} were performed in a few hours on an 12 cores machine clocked at 3.5Ghz and 256GB of RAM. The computations for G_1 took 52 hours on the same machine.

We underline that the precision for the computation of the elements of the triangle (points and angles) is always close to machine precision (between 10^{-12} and 10^{-16}), while for the eigenvalues we have 8 digits of precision for the finite groups case and 6 digits of precision for the infinite group case. Even though we have limited precision, this study allows us to make a clear classification of models with respect to eigenvalues for the finite groups. For the infinite groups we manage to observe connections between the combinatorial group and the symmetry group of the associated triangle.

We manage to identify surprising non-Hadamard cases where the associated triangle has two right angles and therefore, its fundamental eigenvalue and exponent can be computed explicitly. Moreover, if we want to have more precision for a particular model, it is possible to compute explicitly the components of the triangle and find the fundamental eigenvalue and the exponent close to machine precision. For example, we found that the eigenvalue of the triangle associated to the Kreweras model is

$$\lambda_1 = 5.159\,145\,642\,470,$$

where we believe that all digits present are correct. This is very close to the result of Guttmann [42].

7. MISCELLANEOUS

7.1. Other cones. As we have seen throughout the article, computing critical exponents for walks in the cone \mathbb{N}^3 (or in any cone formed by an intersection of three half-spaces, by a linear transform) requires the computation of the principal eigenvalue of a spherical triangle.

More generally, we could consider walks confined to an arbitrary cone K in dimension 3 or more (even so the natural and fruitful combinatorial interpretation of positive walks is lost), and ask whether there exists a closed-form expression for the principal eigenvalue. However, only very few domains seem to admit such closed-form eigenvalues. Besides spherical digons and birectangle triangles, there are for instance the revolution cones, see Figure 17. The first eigenvalue (and in fact the whole spectrum) is described in Lemma 24 of Section A.2 in the appendix.

From an analytic viewpoint, the domains leading to explicit eigenvalues have typically the property of separation of the variables, see [53, 54] for more details.

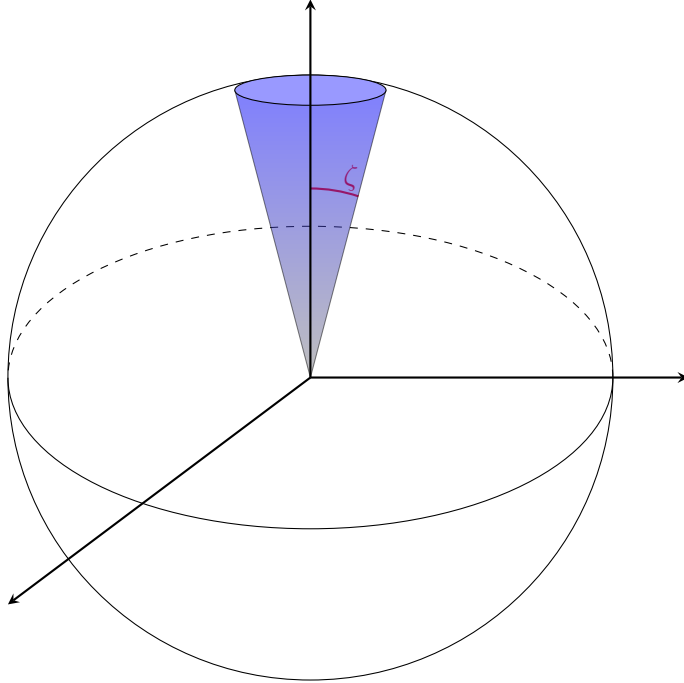


FIGURE 17. The revolution cone (or spherical cap) $K(\zeta)$ of apex angle ζ

7.2. Total number of walks. Throughout the article we have considered the asymptotics of the number of excursions (essentially, the coefficients of $O(0, 0, 0; t)$, see (1) and (2)), but other questions are relevant from an enumerative combinatorics viewpoint, as the asymptotics of the total number of walks (regardless of the ending position), or equivalently the coefficients of the series $O(1, 1, 1; t)$.

Let us recall that it is still an open problem to determine, in general, the asymptotics as $n \rightarrow \infty$ of the coefficients of $O(1, 1, 1; t)$. Assume that it has the form

$$[t^n]O(1, 1, 1; t) = \varkappa \cdot \rho^n \cdot n^{-\beta} \cdot (1 + o(1)). \quad (36)$$

Recall from [40] that under the hypothesis (H), there exists $(x^*, y^*, z^*) \in [1, \infty)^3$ such that

$$\min_{[1, \infty)^3} \chi = \chi(x^*, y^*, z^*),$$

and then the exponential growth ρ in (36) is given by $\rho = \chi(x^*, y^*, z^*)$; compare with (15). There are essentially three cases for which the critical exponent β in (36) is known:

- Case of a drift in the interior of \mathbb{N}^3 ($\beta = 0$);
- Zero drift (then $\beta = \frac{\lambda}{2} - \frac{3}{4}$, λ being the critical exponent of the excursions (2));
- Case when the point (x^*, y^*, z^*) is in the interior of the domain $[1, \infty)^3$, i.e., $x^* > 1$, $y^* > 1$ and $z^* > 1$ (in that case $\beta = \lambda$).

In the first case (drift with positive entries), the exponent is obviously 0 by the law of large numbers.

In the second case the exponent β is given by the formula (32) proved in [29]. As recalled in (31), β is a simple affine combination of λ , namely $\beta = \frac{\lambda}{2} - \frac{3}{4}$.

The last case is proved by Duraj in [32]. The original statement of Duraj is in terms of the minimum of the Laplace transform of the step set on the dual cone, but it is equivalent to the one presented above, after an exponential change of variables and using that the

octant \mathbb{N}^3 is self-dual. The hypothesis that the point (x^*, y^*, z^*) is an interior point cannot be easily translated in terms of the drift; note, however, that it contains the case of a drift with three negative coordinates. The intuition of the formula $\beta = \lambda$ is that the drift being directed towards the vertex of the cone, a typical walk will end at a point close to the vertex, and thus asymptotically the total number of walks is comparable to the number of excursions.

Among the more than 11 millions of models, there are of course many examples corresponding to each of the above cases.

7.3. Walks in the quarter plane and spherical digons. In this paragraph we would like to briefly explain how the more classical model of walks in the quarter plane enters into the framework of spherical geometry. In one sentence, spherical triangles become degenerate and should be replaced by spherical digons, see Figure 18, for which the principal eigenvalue is known.

Indeed, given a 2D positive random walk $\{(X(n), Y(n))\}$, we can choose an arbitrary 1D random walk $\{Z(n)\}$ and embed the 2D model as a 3D walk $\{(X(n), Y(n), Z(n))\}$, with no positivity constraint on the last coordinate. The natural cone is therefore $\mathbb{N}^2 \times \mathbb{Z}$, or after the decorrelation of the coordinates, the cartesian product of a wedge of opening α and \mathbb{Z} . On the sphere \mathbb{S}^2 , the section of the latter domain is precisely a spherical digon of angle α .

Moreover, the smallest eigenvalue λ_1 of a spherical digon is easily computed, see, e.g., [56, Sec. 5]:

$$\lambda_1 = \frac{\pi}{\alpha} \left(\frac{\pi}{\alpha} + 1 \right).$$

The formula (5) relating the smallest eigenvalue to the critical exponent gives an exponent equal to $\frac{\pi}{\alpha} + \frac{3}{2}$. To find the exponent of the initial planar random walk we have to subtract $\frac{1}{2}$ (exponent of an unconstrained excursion in the z -coordinate), which by [29, 18] is the correct result.

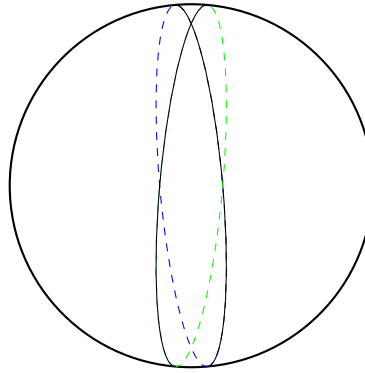


FIGURE 18. A spherical digon is the domain bounded by two great arcs of circles

7.4. Exit time from cones for Brownian motion. As shown in [28, 6] (see in particular [6, Cor. 1]), the exit time of a standard d -dimensional Brownian motion from a cone K behaves when $t \rightarrow \infty$ as

$$\mathbb{P}_x[\tau > t] = B_1 \cdot m_1 \left(\frac{x}{|x|} \right) \cdot \left(\frac{|x|^2}{2} \right)^{\lambda_1(K)/2} \cdot t^{-\lambda_1(K)/2}, \quad (37)$$

where $\lambda_1(K)$ is equal to

$$\lambda_1(K) = \sqrt{\lambda_1(C) + \left(1 - \frac{d}{2}\right)^2 + \left(1 - \frac{d}{2}\right)}$$

and $\lambda_1(C)$ is the principal eigenvalue of the Dirichlet problem on the section $C = K \cap \mathbb{S}^{d-1}$:

$$\begin{cases} \Delta_{\mathbb{S}^{d-1}} m = -\Lambda m & \text{in } C, \\ m = 0 & \text{in } \partial C. \end{cases} \quad (38)$$

In the asymptotics (37), m_1 is the (suitably normalized) eigenfunction associated to λ_1 .

In the particular case of 3D Brownian motion, if the cone K is an intersection of three half-spaces, the section C becomes a spherical triangle and the exponent in (37) is directly related to the principal eigenvalue of a spherical triangle, which is the main object of investigation studied in this paper.

Let us finally comment on the case of non-standard Brownian motion (in arbitrary dimension $d \geq 2$). First, the case of non-identity covariance matrices is easily reduced to the standard case, by applying a simple linear transform (notice, however, that this implies changing the initial cone, and therefore the domain of the Dirichlet problem). The situation is more subtle in the case of drifted Brownian motion: various asymptotic regimes exist, depending on the position of the drift with respect to the cone and the polar cone [39]. In some regimes the exponent in (37) involves the principal eigenvalue λ_1 ; in some other cases (e.g., a drift which belongs to the interior of the cone) the exponent is independent of the geometry of the cone.

7.5. Other methods to approximate the first eigenvalue. We have developed in Section 6 a finite element method to compute precise approximations of the first eigenvalue. We would like to briefly mention here two alternative approaches.

First, using the stereographic projection, the 3D eigenvalue problem (6) can be rewritten as a 2D eigenvalue problem for a different operator. Since the stereographic projection maps circles onto circles, the new domain is bounded by three arcs of circles and is thus rather simple. Moreover, this technique has the obvious advantage to work with two variables instead of three. However, as expected, the eigenvalue problem becomes more complicated and is not exactly solvable. See [37, 36] for more details (in particular [36, Eq. (2.12) and Fig. 3]).

Finally, the authors of [51] describe a Monte Carlo method for the numerical computation of the first eigenvalue of the Laplace operator in a bounded domain with Dirichlet conditions. It is based on the estimation of the speed of absorption of the Brownian motion by the boundary of the domain. Theoretically this could certainly be used in our situation, but as many probabilistic methods, it is hard to expect a precision such as ours (typically, ten digits).

7.6. Open problems. Besides the open problems listed in Section 9 of [13], let us mention the following:

Singularity analysis. Is this possible to obtain similar results on non-D-finiteness of Hadamard models using the Hadamard product of generating functions? See Corollaries 8 and 13 as well as Section 4.3.

3D Kreweras model. This is clearly the case for which we can find the greatest number of estimations in the literature. Let us quickly give a chronological list (probably non-exhaustive):

- [5.15, 5.16] by Costabel (2008, [26])
- 5.159 by Ratzkin and Treibergs (2009, [53, 54])
- 5.1589 by Bostan, Raschel and Salvy (2012, [17])
- 5.162 by Balakrishna (2013, [3])
- 5.1606 by Balakrishna (2013, [4])
- 5.1591452 by Bacher, Kauers and Yatchak (2016, [2])
- 5.159145642466 Guttmann (2017, [42])
- 5.159145642470 by our result

What is the exact value? Is it a rational number?

REFERENCES

- [1] C. Alves and P. Antunes (2018) The method of fundamental solution applied to boundary value problems on the surface of a sphere. *Comput. Math. Appl.* **75** 2365–2373
- [2] A. Bacher, M. Kauers and R. Yatchak (2016). Continued classification of 3D lattice models in the positive octant. *Proceedings of FPSAC'16, DMTCS* 95–106
- [3] B. Balakrishna (2013). Heat Equation on the Cone and the Spectrum of the Spherical Laplacian. *Preprint arXiv:1301.6202v3*, 1–16
- [4] B. Balakrishna (2013). On multi-particle Brownian survivals and the spherical Laplacian. *Preprint* available at this http url
- [5] C. Banderier and P. Flajolet (2002). Basic analytic combinatorics of directed lattice paths. *Theoret. Comput. Sci.* **281** 37–80
- [6] R. Bañuelos and R. Smits (1997). Brownian motion in cones. *Probab. Theory Related Fields* **108** 299–319
- [7] P. Bérard (1983). Remarques sur la conjecture de Weyl. *Compositio Math.* **48** 35–53
- [8] P. Bérard and G. Besson (1980). Spectres et groupes cristallographiques. II. Domaines sphériques. *Ann. Inst. Fourier* **30** 237–248
- [9] M. Berger (1987). *Geometry. II.* Translated from the French by M. Cole and S. Levy. Universitext. Springer-Verlag, Berlin
- [10] J. Bertoin and R. Doney (1994). On conditioning a random walk to stay nonnegative. *Ann. Probab.* **22** 2152–2167
- [11] B. Bogosel (2016). The method of fundamental solutions applied to boundary eigenvalue problems. *J. Comput. Appl. Math.* **306** 265–285
- [12] F. Bornemann, D. Laurie, S. Wagon and J. Waldvogel (2004). The SIAM 100-digit challenge. *SIAM, Philadelphia PA*
- [13] A. Bostan, M. Bousquet-Mélou, M. Kauers and S. Melczer (2016). On 3-dimensional lattice walks confined to the positive octant. *Ann. Comb.* **20** (2016), no. 4, 661–704
- [14] A. Bostan, M. Bousquet-Mélou and S. Melczer (2018). On walks with large steps in an orthant. *Preprint*
- [15] A. Bostan and M. Kauers (2009). Automatic classification of restricted lattice walks. *Proceedings of FPSAC'09, DMTCS* 201–215
- [16] A. Bostan and M. Kauers (2010). The complete generating function for Gessel walks is algebraic. *Proc. Amer. Math. Soc.* **138** 3063–3078. With an appendix by Mark van Hoeij
- [17] A. Bostan, K. Raschel and B. Salvy (2012). Unpublished notes.
- [18] A. Bostan, K. Raschel and B. Salvy (2014). Non-D-finite excursions in the quarter plane. *J. Combin. Theory Ser. A* **121** 45–63
- [19] N. Bourbaki (1968). *Éléments de mathématique. Fasc. XXXIV. Groupes et algèbres de Lie.* Actualités Scientifiques et Industrielles, No. 1337 Hermann
- [20] M. Bousquet-Mélou (2016). Square lattice walks avoiding a quadrant. *J. Combin. Theory Ser. A* **144** 37–79
- [21] M. Bousquet-Mélou and M. Mishna (2010). Walks with small steps in the quarter plane. *Algorithmic probability and combinatorics* 1–39, Contemp. Math., **520**, Amer. Math. Soc., Providence, RI

- [22] I. Chavel (1984). *Eigenvalues in Riemannian geometry*. Pure and Applied Mathematics, **115**. Academic Press, Inc., Orlando, FL
- [23] J. Cohen (1984). On a functional relation in three complex variables; three coupled processors. *Technical Report Mathematical Institute Utrecht 359*, Utrecht University
- [24] P. D'Arco, V. Lacivita and S. Mustapha (2016). Combinatorics meets potential theory. *Electron. J. Combin.* **23** Paper 2.28, 17 pp
- [25] M. Dauge (1988). *Elliptic boundary value problems on corner domains. Smoothness and asymptotics of solutions*. Lecture Notes in Mathematics, 1341. Springer-Verlag, Berlin
- [26] M. Dauge (2017). Private communication.
- [27] A. Davydychev and R. Delbourgo (1998). A geometrical angle on Feynman integrals. *J. Math. Phys.* **39** 4299–4334
- [28] R. DeBlassie (1987). Exit times from cones in \mathbb{R}^n of Brownian motion. *Probab. Theory Related Fields* **74** 1–29
- [29] D. Denisov and V. Wachtel (2015). Random walks in cones. *Ann. Probab.* **43** 992–1044
- [30] T. Dreyfus, C. Hardouin, J. Roques and M. Singer (2018). On the nature of the generating series of walks in the quarter plane. *Invent. Math.* (to appear)
- [31] D. Du, Q.-H. Hou and R.-H. Wang (2016). Infinite orders and non-D-finite property of 3-dimensional lattice walks. *Electron. J. Combin.* **23** no. 3, Paper 3.38, 15 pp
- [32] J. Duraj (2014). Random walks in cones: the case of nonzero drift. *Stochastic Process. Appl.* **124** 1503–1518
- [33] J. Duraj and V. Wachtel (2015). Invariance principles for random walks in cones. *Preprint arXiv:1508.07966* 1–17
- [34] G. Dziuk and C. Elliott (2013). Finite element methods for surface PDEs. *Acta Numer.* **22** 289–396
- [35] G. Fayolle, R. Iasnogorodski and V. Malyshev (1999). *Random walks in the quarter-plane. Algebraic methods, boundary value problems and applications*. Applications of Mathematics (New York), 40. Springer-Verlag, Berlin
- [36] G. Fichera (1973/74). Comportamento asintotico del campo elettrico e della densità elettrica in prossimità dei punti singolari della superficie conduttrice. *Rend. Sem. Mat. Univ. e Politec. Torino* **32** 111–143
- [37] G. Fichera and M. Sneider (1974). Distribution de la charge électrique dans le voisinage des sommets et des arêtes d'un cube. *C. R. Acad. Sci. Paris Sér. A* **278** 1303–1306
- [38] G. Fix (1973). Eigenvalue approximation by the finite element method. *Advances in Math.* **10** 300–316
- [39] R. Garbit and K. Raschel (2014). On the exit time from a cone for Brownian motion with drift. *Electron. J. Probab.* **19** no. 63 1–27
- [40] R. Garbit and K. Raschel (2016). On the exit time from a cone for random walks with drift. *Rev. Mat. Iberoam.* **32** 511–532
- [41] T. Guttmann (Editor) (2009). *Polygons, polyominoes and polycubes*. Lecture Notes in Physics, 775. Springer, Dordrecht
- [42] T. Guttmann (2017). Private communication.
- [43] A. Henrot and M. Pierre (2005). *Variation et optimisation de formes*, Mathématiques & Applications. Springer, Berlin
- [44] L. Hillairet and C. Judge (2009). Generic spectral simplicity of polygons. *Proc. Amer. Math. Soc.* **137** 2139–2145
- [45] G. Kanschat (2017). Finite element methods for variational eigenvalue problems. *Contemp. Math.* **700**
- [46] T. Kato (1976). Perturbation theory for linear operators. Springer-Verlag, Berlin-New York.
- [47] M. Kauers (2017). Private communication.
- [48] M. Kauers and R.-H. Wang (2017). Lattice walks in the octant with infinite associated groups. *Proceedings of EUROCOMB 2017, Electronic Notes in Discrete Mathematics* **61** 703–709
- [49] M. Kauers and R. Yatchak (2015). Walks in the quarter plane with multiple steps. *Proceedings of FPSAC'15, DMTCS* 25–36
- [50] I. Kurkova and K. Raschel (2012). On the functions counting walks with small steps in the quarter plane. *Publ. Math. Inst. Hautes Études Sci.* **116** 69–114
- [51] A. Lejay and S. Maire (2007). Computing the principal eigenvalue of the Laplace operator by a stochastic method. *Math. Comput. Simulation* **73** 351–363
- [52] L. Lipshitz (1988). The diagonal of a D-finite power series is D-finite. *J. Algebra* **113** 373–378
- [53] J. Ratzkin and A. Treibergs (2009). A Payne-Weinberger eigenvalue estimate for wedge domains on spheres. *Proc. Amer. Math. Soc.* **137** 2299–2309

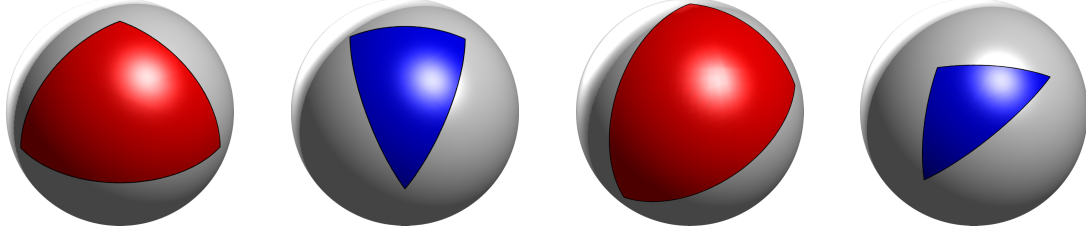


FIGURE 19. Two triangles (color red) and their polar triangles (in blue), see Definition 20

- [54] J. Ratzkin and A. Treibergs (2009). A capture problem in Brownian motion and eigenvalues of spherical domains. *Trans. Amer. Math. Soc.* **361** 391–405
- [55] H. Schwarz (1873). Ueber diejenigen Fälle, in welchen die Gaussische hypergeometrische Reihe eine algebraische Function ihres vierten Elementes darstellt. *J. Reine Angew. Math.* **75** 292–335
- [56] H. Walden (1974). *Solution of an eigenvalue problem for the Laplace operator on a spherical surface*. Document No. X-582-74-41, NASA/Goddard Space Flight Center
- [57] H. Walden and R. Kellogg (1977). Numerical determination of the fundamental eigenvalue for the Laplace operator on a spherical domain. *J. Engrg. Math.* **11**, no. 4, 299–318
- [58] R. Yatchak (2017). Automated positive part extraction for lattice path generating functions in the octant. *Proceedings of EUROCOMB 2017, Electronic Notes in Discrete Mathematics* **61** 1061–1067

APPENDIX A. SOME USEFUL DEFINITIONS FROM SPHERICAL GEOMETRY

A.1. Elementary spherical geometry. Our main source is the book [9] by Berger. Spherical triangles have been introduced in Definition 2. A spherical digon as on Figure 18 is a domain bounded by two great arcs of circles, see [9, 18.3.8.2].

A natural operation in spherical geometry is to take the polar spherical triangle; see [9, 18.3.8.2] and [9, 18.6.12] for more details.

Definition 20 (polar triangle). *Let $\langle x, y, z \rangle$ be a spherical triangle in the sense of Definition 2. Define the triplet (x', y', z') by the conditions*

$$\begin{cases} \langle x', y \rangle = \langle x', z \rangle = 0, & \langle x', x \rangle > 0, \\ \langle y', z \rangle = \langle y', x \rangle = 0, & \langle y', y \rangle > 0, \\ \langle z', x \rangle = \langle z', y \rangle = 0, & \langle z', z \rangle > 0. \end{cases}$$

Then $\langle x', y', z' \rangle$ is a spherical triangle, called the polar triangle of $\langle x, y, z \rangle$.

This transformation is involutive, and the equilateral right triangle is invariant. There is no simple formula relating the eigenvalues of a spherical triangle to that of its polar triangle. See Figure 19 for examples.

Interestingly, polar cones already appear in [40] (resp. [39]) to compute the exponential decay of the survival probability of random walks (resp. the exponential decay and the critical exponent of the Brownian survival probability) in cones.

A.2. Some properties of the principal eigenvalue. Our main reference here is the book [25] of Dauge.

Monotonicity and regularity of the eigenvalues.

Lemma 21 (Lemma 18.5 in [25]). *Let T_1 and T_2 be two simply connected domains on \mathbb{S}^2 . If $T_1 \subset T_2$ then*

$$\lambda_1(T_1) \geq \lambda_1(T_2).$$

In particular, as any spherical triangle is included in a half-sphere (whose principal eigenvalue equals 2), one has the natural and universal lower bound

$$\lambda_1(T) \geq 2$$

for any spherical triangle T . (By (5), this implies that the critical exponent λ should be bigger than $\frac{5}{2}$.)

Classical arguments in perturbation theory for operators [46] state that analytic perturbations of the operator induce analytic perturbations of the eigenvalues, see in particular [44, Lem. 2.1] in our context. It is possible to find an explicit expression of the first derivative of the eigenvalue using results from [43].

Lemma 22. *The function $\lambda_1(T) = \lambda_1(\alpha, \beta, \gamma)$ is analytic in the angles α, β, γ .*

A consequence of Lemma 22 is that a generic triangle has a non-rational principal eigenvalue λ_1 .

Lemma 23. *As one of the angles goes to 0, λ_1 goes to infinity.*

Proof. Lemma 23 is a simple consequence of Lemma 21 and the fact that each spherical triangle can be included in any of the digons determined by its angles. Indeed, suppose the triangle T has an angle equal to α . Then T is included in the digon D_α with angle α and

$$\lambda_1(T) \geq \lambda_1(D_\alpha) = \frac{\pi}{\alpha} \left(\frac{\pi}{\alpha} + 1 \right).$$

We can notice immediately that if $\alpha \rightarrow 0$ then the first eigenvalue of T goes to infinity. \square

Revolution cones. We now compute the spectrum of a revolution cone (or solid angle) in arbitrary dimension $d \geq 2$. Introduce some notation. We fix a half-axis A in \mathbb{R}^d and for any $x \neq 0$ denote by $\theta(x) \in [0, \pi]$ the angle between the axes A and \vec{x} . By definition, the revolution cone with apex angle ζ is (see Figure 17)

$$K(\zeta) = \{x \in \mathbb{R}^d \setminus \{0\} : \theta(x) \in (0, \zeta)\}. \quad (39)$$

Its section on the sphere is the circle $C(\zeta) = K(\zeta) \cap \mathbb{S}^2$.

Lemma 24 (Proposition 18.10 in [25]). *The spectrum of $C(\zeta)$ is the set of positive $\nu(\nu + d - 2)$ for which there is $m \in \mathbb{N}$ such that $P_\nu^m(\cos \zeta) = 0$, where P_ν^m denotes the m th Legendre function of the first kind.*

Notice that [25, Proposition 18.10] computes the spectrum of the cone $K(\zeta)$, not of its section $C(\zeta)$. However the eigenvalues $\lambda_i(K)$ of a cone K are strongly related to the eigenvalues of its section $C = K \cap \mathbb{S}^2$, namely (see, e.g., [25, 18.3])

$$\lambda_i(K) = \sqrt{\lambda_i(C) + \left(1 - \frac{d}{2}\right)^2} + \left(1 - \frac{d}{2}\right). \quad (40)$$

A few remarkable spherical triangles. Consider triangles with angles

$$\left(\frac{\pi}{p}, \frac{\pi}{q}, \frac{\pi}{r} \right), \quad \text{with } p, q, r \in \mathbb{N} \setminus \{0, 1\}.$$

As recalled in [7, 25], the only possible triplets are

- (2, 3, 3) tetrahedral group
- (2, 3, 4) octahedral group
- (2, 3, 5) icosahedral group
- (2, 2, r) dihedral group or order $2r \geq 4$

Each triplet above corresponds to a tiling of the sphere. See Figures 6 and 11 for a few examples. Denote by $T_{(p,q,r)}$ the associated triangle when it exists.

Lemma 25 (Theorem 6 in [7]). *The eigenvalues of $T_{(p,q,r)}$ have the form $\nu_{(p,q,r)}(\nu_{(p,q,r)}+1)$, with $(\ell_1, \ell_2 \in \mathbb{N})$*

- $\nu_{(2,3,3)} = 6 + 3\ell_1 + 4\ell_2$
- $\nu_{(2,3,4)} = 9 + 6\ell_1 + 6\ell_2$
- $\nu_{(2,3,5)} = 15 + 6\ell_1 + 10\ell_2$
- $\nu_{(2,2,r)} = r + 1 + 2\ell_1 + r\ell_2$

APPENDIX B. REMARKS ON THE EXPONENT OF MIXINGS OF TWO LAWS

Take a random walk in 2D with jumps $(p_{i,j})$. Introduce the (weighted) inventory

$$\chi_p(x, y) = \sum p_{i,j} x^i y^j.$$

Define (x_0, y_0) as the unique solution to $\frac{\partial \chi}{\partial x} = \frac{\partial \chi}{\partial y} = 0$. Then, introduce the new jumps

$$p_{i,j}^0 = p_{i,j} \frac{x_0^i y_0^j}{\chi(x_0, y_0)}.$$

By construction the new jumps have zero drift. Define the correlation factor

$$\text{cor}_p = \frac{\frac{\partial^2 \chi}{\partial x \partial y}}{\sqrt{\frac{\partial^2 \chi}{\partial x^2} \frac{\partial^2 \chi}{\partial y^2}}}(x_0, y_0) = \frac{\sum i j p_{i,j}^0}{\sqrt{\sum i^2 p_{i,j}^0 \cdot \sum j^2 p_{i,j}^0}}.$$

The exponent of the excursion sequence is

$$\lambda_p = \frac{\pi}{\arccos(-\text{cor}_p)} + 1.$$

Consider now two step sets $(p_{i,j})$ and $(q_{i,j})$. Their mixing, with $t \in [0, 1]$, is $(m_{i,j})$ given by

$$m_{i,j} = t p_{i,j} + (1-t) q_{i,j}.$$

Assume that the critical point (x_0, y_0) is the same for $(p_{i,j})$ and $(q_{i,j})$. Then it is also that of m , which has the correlation factor

$$\text{cor}_m = \frac{t \sum i j p_{i,j}^0 + (1-t) \sum i j q_{i,j}^0}{\sqrt{(t \sum i^2 p_{i,j}^0 + (1-t) \sum i^2 q_{i,j}^0) \cdot (t \sum j^2 p_{i,j}^0 + (1-t) \sum j^2 q_{i,j}^0)}}. \quad (41)$$

If the models $(p_{i,j})$ and $(q_{i,j})$ have the same variances

$$u = \sum i^2 p_{i,j}^0 = \sum i^2 q_{i,j}^0, \quad v = \sum j^2 p_{i,j}^0 = \sum j^2 q_{i,j}^0$$

then the formula (41) reduces to

$$\text{cor}_m = t \text{cor}_p + (1-t) \text{cor}_q.$$

E-mail address: benjamin.bogosel@cmap.polytechnique.fr

E-mail address: vincent.perrollaz@lmpt.univ-tours.fr

E-mail address: raschel@math.cnrs.fr

E-mail address: amelie.trotignon@lmpt.univ-tours.fr